Improving the accuracy of atomistic simulations of the electrochemical interface

Ravishankar Sundararaman,[*,†] Derek Vigil-Fowler,[*,‡] and Kathleen Schwarz[*,¶]

†*Department of Materials Science and Engineering, Rensselaer Polytechnic Institute, 110 8th St., Troy, New York 12180, United States*

‡*Materials and Chemical Science and Technology Center, National Renewable Energy Laboratory, Golden, Colorado 80401, United States*

¶*Material Measurement Laboratory, National Institute of Standards and Technology, 100 Bureau Dr., Gaithersburg, Maryland 20899, United States*

E-mail: sundar@rpi.edu; Derek.Vigil-Fowler@nrel.gov; kas4@nist.gov

Abstract

Atomistic simulation of the electrochemical double layer is an ambitious undertaking, requiring quantum mechanical description of electrons, phase space sampling of liquid electrolytes, and equilibration of electrolytes over nanosecond timescales. All models of electrochemistry make different trade-offs in the approximation of electrons and atomic configurations, from the extremes of classical molecular dynamics of a complete interface with point-charge atoms to correlated electronic structure methods of a single electrode configuration with no dynamics or electrolyte. Here, we review the spectrum of simulation techniques suitable for electrochemistry, focusing on the key approximations and accuracy considerations for each technique. We discuss promising approaches, such as enhanced sampling techniques for atomic configurations and computationally-efficient beyond density functional theory (DFT) electronic methods, that will push electrochemical simulations beyond the present frontier.

TOC figure:

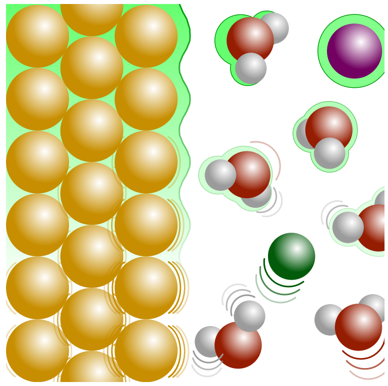

Contents

1 Introduction

Electrochemistry exploits the complex interface of two charge reservoirs – electrons and ions – to facilitate chemical reactions involving electron transfers. Processes at the electrochemical interface involve time and length scales substantially larger than the atomic scale,[1] making atomistic and first-principles modeling of electrochemistry particularly challenging.[2]

Further, accurate simulation of electrons and ions each introduce independent computational costs that necessitate trade-offs between accuracy in electronic structure and sampling of atomic configurations. For example, the electronic charge distribution at a solid-liquid interface requires electronic structure methods that precisely account for the electronic level alignment across the interface, while the most commonly-employed density-functional theory (DFT) methods are not generally accurate for such interfacial alignments.[3–7] Simultaneously, the ionic charge distribution within the electrolyte equilibrates at nanosecond time scales,[1,8,9] which would correspond to millions of time steps in molecular dynamics simulations.

This requires computational electrochemists to make a choice: allocate available resources to adopt an accurate electronic structure method for a few atomic configurations, or sample a large number of atomic configurations using a method with no or low-level electronic structure, *e.g.*, classical molecular dynamics (MD) or *ab initio* MD (AIMD).

This review aims to bring together computational electrochemical techniques ranging from classical MD to first-principles reaction modeling within a unified perspective of improving accuracy of electrochemical simulations, from atomic-configuration sampling to electronic structure. We identify key considerations for accuracy across different methods within this spectrum, outline the choices currently made by typical approaches within computational electrochemistry, and discuss promising techniques that may lead to improved choices in the accuracy trade off.

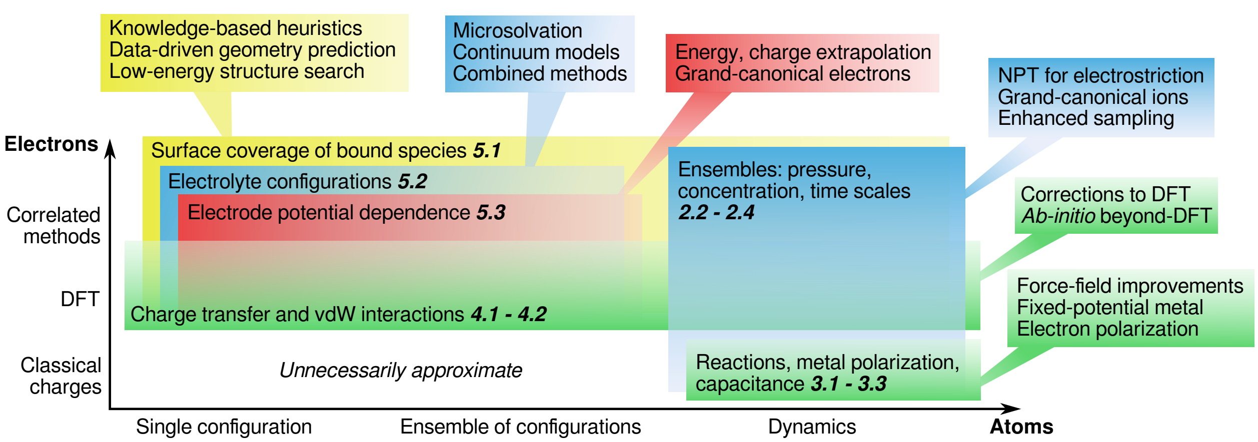

Figure 1: Approximations in computational electrochemistry organized by electronic structure accuracy (y axis) and degree of atomic-configuration sampling (x axis), consequent considerations for accuracy (sticky notes with review section numbers), and typical solutions (call-out boxes). The gradient across a sticky note indicates where each accuracy consideration is most important. The gradient across a sticky note indicates where each accuracy consideration is most important.

Figure 1 categorizes electrochemical simulations by the approaches used for describing electronic structure (electron axis) and atomic-configuration sampling (atom axis). We restrict our focus to within the Born-Oppenheimer approximation, where these axes are independent; see Ref. 10 for a discussion of effects beyond this approximation in electrochemistry. The electron axis ranges from electron-less classical-charge methods to correlated wavefunction and many-body perturbation theory methods. Sampling of atomic configurations ranges from single static configurations, through ensembles of few static configurations, to ensembles sampled by full atomic dynamics (using e.g., an MD method). Computational cost increases away from the origin along both the electron and atom axes, leading typically to a few configurations for high-level electronic methods, and to a low-level electronic description for large ensembles and dynamics methods.

We organize this review by the most important considerations for accuracy across multiple techniques on this electron-atom trade-off spectrum (Figure 1). Specifically, we discuss sampling the appropriate ensemble for the liquid and electrolyte (blue boxes), electronic structure accuracy (green boxes), adequately sampling surface-bound species (yellow box), and accounting for electrode potential effects (red box). We limit coverage to considerations that require a trade off. For example, we focus on electrode potential effects in the single / few configuration case rather than in the case of explicit configuration sampling using MD, where established techniques exist to maintain the electrode potential[7,11–15] and connect it to experimental reference electrodes.[7,13,14,16] We also exclude discussion of electrification and solvation within first-principles electrochemical calculations covered extensively in previous reviews by ourselves[2] and others.[17] Finally, each box in Figure 1 is graded in intensity to indicate where each consideration is most important, and points to the sections that discuss it.

2 Computational setup for dynamics

The goals of electrochemical simulations span a wide range from predicting physical properties of the electrochemical interface, such as capacitance, to predicting mechanisms of chemical reactions at the interface. Correspondingly, the computational setup of such simulations varies widely. At one extreme, reaction mechanism calculations may focus on the energy landscape of molecules adsorbed at an electrode surface, eliminating the electrolyte atoms entirely or replacing their effect with a continuum approximation (top left region of Figure 1). Explicitly including the liquid/electrolyte structure in electrochemical simulations requires techniques to sample the thermodynamic phase space of atomic configurations, typically achieved with molecular dynamics (MD) simulations (right region of Figure 1).

We begin with common considerations for all MD methods that explicitly simulate atomic motion using an approximation of the potential energy and forces for each atomic configuration. These include lower-cost classical MD methods that employ empirical force fields, approximated directly as a function of atomic positions (Section 3), and more expensive *ab initio* MD (AIMD) methods that derive forces from electronic structure calculations (Section 4) of each atomic configuration. Classical MD calculations for electrochemistry typically simulate $10^3 - 10^4$ atoms over few-to-tens of nanometer dimensions for $1 - 10$ nanoseconds, while AIMD simulations typically simulate ~ 100 atoms over few nanometer dimensions for $10 - 100$ picoseconds. Within these computational constraints, MD simulations of electrochemical double layers must be sufficiently long to properly equilibrate *and* simultaneously large enough to maintain a region with bulk electrolyte concentration and pressure, as we discuss next.

2.1 Choice of simulation cell for molecular dynamics

Molecular dynamics simulation cells for electrochemistry can include two oppositely-charged electrodes,[18] or one or two half cells with a single electrode charge,[19] as illustrated by Figure 2. The full-cell approach (Figure 2(a)) is convenient for rapidly evaluating the dependence of interface properties as a function of charge or potential, since it provides quantities for both positive and negatively charged electrodes from each simulation. While this approach is common in larger classical MD simulations, it requires care in smaller simulation cells with few ions. Depending on the electrode charge, the expected equilibrium profile for a full-cell simulation could necessitate fractional numbers of ions in each half cell, which would then impractically require ions to diffuse between the two halves repeatedly within the time scale of the simulation (Section 2.3). Additionally, these simulation cells involve a finite electric field, which require careful treatment of polarization in AIMD simulations.[20]

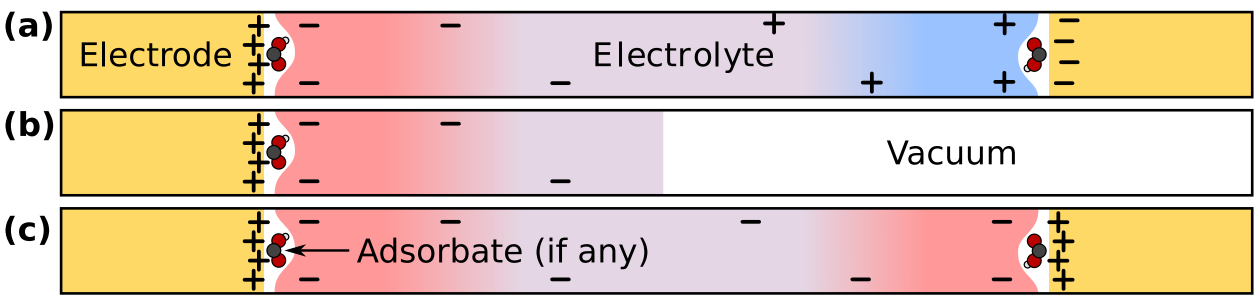

Figure 2: Electrochemical simulation cells can target (a) a full cell with oppositely-charged electrodes, (b) a single half cell with a vacuum interface, or (c) back-to-back half-cells with the same electrode charge. The electrode and adsorbate regions are typically modeled atomistically, while the electrolyte region could be described atomistically, as a continuum or a combination thereof. Atomistic modeling could employ force fields or electronic structure methods, on a single atomic configuration or several configurations sampled by e.g., molecular dynamics.

Half-cell simulations are more typical for AIMD simulations, a consequence of their necessarily smaller and shorter runs.[19] Such calculations explicitly ensure a balance between the electrode and ionic charges, avoiding the potential issue of requiring ions to straddle two half cells discussed above. Further, half cell simulations could either employ a single half cell combined with a electrolyte-vacuum interface (Figure 2(b)), or two back-to-back half cells of the same electrode charge (Figure 2(c)).[21] The first approach (Figure 2(b)) allows the electrolyte density to equilibrate by moving the interface boundary, avoiding bulk-density issues that can arise in approaches without a vacuum interface (see Section 2.2). However, the atoms and simulation cell space expended for the electrolyte-vacuum interface is not used effectively towards the electrochemical interface of interest. This can be partially mitigated by replacing the vacuum region with a continuum electrolyte, as in the effective screening medium (ESM) setup for AIMD simulations.[12] In contrast, simulations with two back-to-back half cells of the same charge provide statistics for two electrochemical interfaces from each simulation,[21,22] as in the full-cell approach. Additionally, they involve a nominally inversion-symmetric overall simulation cell suitable for use with periodic boundary conditions (typical in AIMD).

2.2 Choice of ensemble in molecular dynamics

The small system size of MD simulations relative to real electrochemical interfaces necessitates special care to faithfully reproduce experimental conditions. The macroscopic bulk electrolyte in experiment serves as a reservoir for solvent and ions at the interface, which effectively sets the pressure and ion chemical potential in the interfacial region.[2] In contrast, electrochemical simulations have a small bulk region that may be strongly affected by the interface, depending on the ensemble employed in the MD simulation. Specifically, simulation in a grand-canonical μPT ensemble, which maintains chemical potential of ions μ and pressure P by varying the number of ions and volume, would most closely mimic the experimental condition. However, MD simulations typically adopt NVT ensembles with fixed number and volume or NPT ensembles with fixed number and pressure for practical considerations, which may lead to deviations of pressure and ionic concentration in small bulk regions as discussed next.

The main reason for difficulties in maintaining appropriate bulk thermodynamic conditions is that the electrolyte-surface interactions strongly modify the electrolyte structure at the interface, especially at charged interfaces with strong electric fields at the electrode surface. These fields lead to an increase in the average density near the interface by electrostriction,[23] thus reducing the molecules available for the bulk within a simulation in the canonical ensemble. Simulations of liquids with a fixed separation between two interfaces (in the NVT ensemble) always require determination of the appropriate number of molecules to target the bulk density. Electrostriction additionally makes the required number of molecules dependent on the surface electric field, and hence on the electrode charge or potential. Electrostriction can be a large effect, and is a significant factor in determining the differential capacitance profile of ionic liquids.[24,25] Similarly, the electric fields at the interface increase the concentration of some ions while suppressing the concentration of oppositely-charged ions, requiring corresponding opposite changes in the bulk region of MD simulations at constant volume and ion number. Such changes in bulk density and concentration may be insignificant in large-enough NVT simulations,[26] but become increasingly important in smaller simulation cells, such as those typical for AIMD.

Switching to constant-pressure (NPT) or grand-canonical ensembles for the solvent and ions would resolve these issues by ensuring that densities and concentrations far from the interface are in equilibrium with the bulk electrolyte, as we discuss below. Despite the widespread availability of NPT, for computational convenience, a vast majority of MD simulations of electrochemistry work in constant volume and number (NVT) ensembles. Changing volumes in NPT simulations would require electrodes whose relative spacing fluctuates during the simulation, making it challenging to analyze electrolyte structure and electrostatic potential profiles relative to the electrode position. Instead, in NVT MD simulations, one can adjust the electrode spacing to get the correct bulk densities in the setup of the simulation, and not change the spacing dynamically during the simulation.[21,27] Alternately, as discussed above in Section 2.1, half-cell simulations with a vacuum interface avoid bulk density issues.[19]

Changes in bulk electrolyte concentration in canonical ensemble simulations potentially pose a more severe issue than density changes at fixed volume. For ionic liquids, concentration and density effects are comparable because the concentration of each ionic species is comparable to the overall number density of the liquid. However, in electrolytes with low concentrations of ions in a solvent, concentration effects are more significant due to the low overall numbers of ions in the bulk region.[1] This can be addressed by switching to grand-canonical simulations, such as by using grand-canonical Monte-Carlo (GCMC) methods that include ion insertion and deletion moves with probabilities set by the chemical potential.[28] The chemical potential of ions is, in turn, set to reproduce the target ionic concentration in the bulk fluid.[28] For electrochemical simulations, grand-canonical molecular dynamics (GCMD) methods that incorporate such insertion/deletion moves within MD simulations are more efficient than GCMC.[29] Such insertion/deletion methods have primarily employed classical force fields due to computational cost. Grand-canonical statistics can be realized in a more limited context with AIMD simulations by combining results from simulations with different ion numbers using weights based on the chemical potential, e.g., to control surface proton concentrations at fixed pH (bulk proton concentrations).[30] Beyond fixing the ionic concentration, it is also important to ensure that the spatial distribution of ions equilibrates within the time scale of the simulation, as we discuss next.

2.3 Time scales

The limited timescale of MD simulations, usually $10 - 100$ ps in AIMD to $1 - 10$ ns in classical MD, necessitates care to ensure adequate sampling of atomic configurations of the electrochemical interface. This is of course most important for the slowest processes, which include rearrangement of strongly-adsorbed species at the electrode surface and ion diffusion in the electrolyte.

Strong adsorption may favor specific low-energy atomic configurations, separated by energy barriers that slow down the dynamics of switching between these configurations and reaching equilibrium. Such strongly-adsorbed species could include molecules undergoing an electrochemical transformation, or even chemisorbed ions or solvent molecules from the electrolyte. For instance, the rotational time scale of water adsorbed at the interface can be much slower than in bulk water[31] and can depend strongly on the electrode potential.[32,33]

The equilibration time for chemisorbed water, *e.g.*, on Pt surfaces, can even exceed 10 ns.[34–36] We discuss approaches to sample such slow-to-equilibrate configurations in Section 2.4.

Additionally, the diffusion of ions in the electrolyte leads to a long time scale of double layer formation.[1,8,9] The electrochemical double layer includes an inner layer of ions within a few Angstroms of the electrode, followed by a diffuse layer of ions that extends from a few Angstroms at high electrolyte concentrations to several nanometers at lower electrolyte concentrations.[2] Consequently, the challenge of equilibrating the double layer increases in severity with decreasing electrolyte concentration, with fewer ions required to diffuse greater distances within the simulation time scales. This is particularly serious in AIMD simulations, where computational costs limit calculations to 100 to 200 atoms, leading to very few ion pairs (often just one) in the simulation cell.

To illustrate possible issues due to diffuse-layer time scales and small ion numbers, Figure 3 shows ion profiles of aqueous NaF electrolyte between electrified Ag(100) electrodes in a typical AIMD-sized cell with 1 ion pair at 54 water molecules, but calculated using classical MD to explicitly check the equilibration time scales. The simulations use SPC/E water[37] and alkali-halide parameters from Ref. 38 in the Large-scale Atomic/Molecular Massively Parallel Simulator (LAMMPS)[39] code in a canonical (NVT) ensemble at 300 K with a 1 fs time step. The electrode is described with fixed atomic charges and interacts with the electrolyte using Morse potentials parameterized to DFT calculations. (See Ref. 21 for details on the force field parameters and potential calculation.) The left panels show the water O and H densities and Na^+ and F^- ion profiles at upper-bound AIMD time scales of 100 ps, averaged over 5 sequential 20 ps chunks. The colors/dashes range from lightest/sparsest to darkest/solid with increasing time of simulation, starting from an initial configuration with ions at the interfacial layer as often employed in AIMD. The water density profiles do not seem to change significantly over this time scale, but the ions are confined to a few Angstrom in z in each 20 ps chunk, and these chunks overall move around at the 100 ps time scale. In contrast, the right panels show a simulation starting from exactly the same configuration

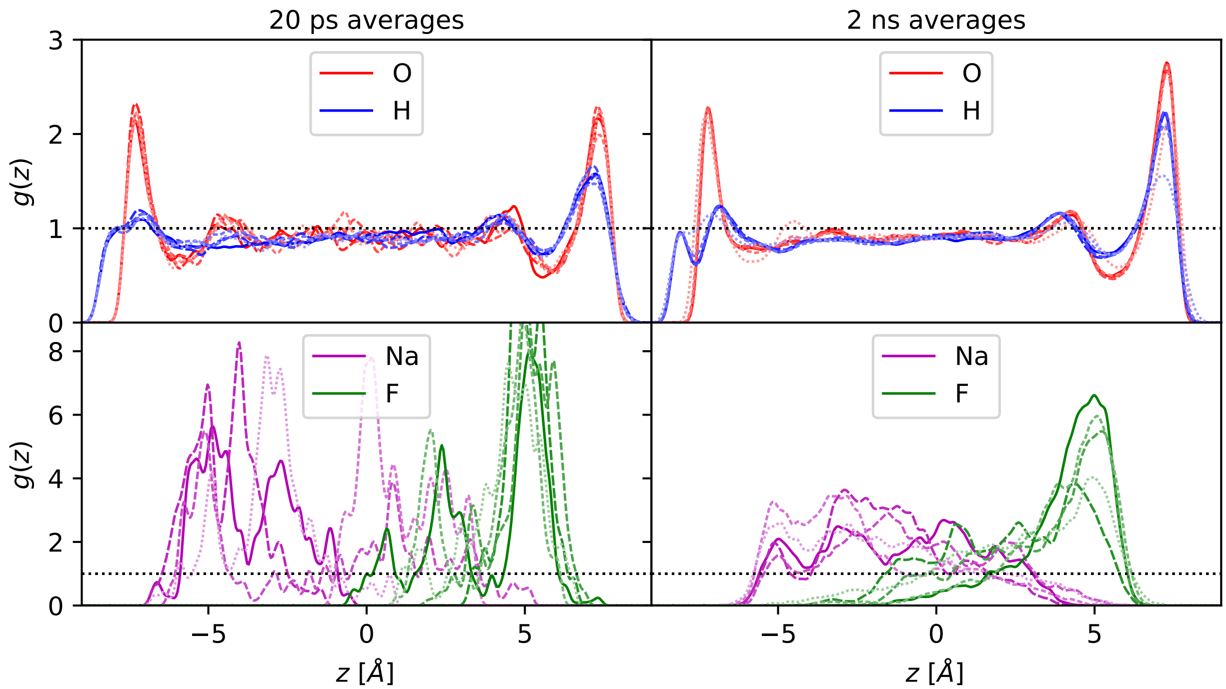

Figure 3: Water and ion density profiles from classical MD simulation of an aqueous 1M NaF electrolyte in a $10 \times 10 \times 20$ Å simulation cell typical for AIMD (contains 54 water molecules and 1 ion pair), between Ag(100) electrodes charged to ± 10 μC/cm^2 (full cell, as in Figure 2(a)). Left panels show results averaged over five sequential 20 ps segments typically feasible in AIMD, while the right panels show averages over 2 ns segments from the same initial configuration (each averaged over 500 equally-spaced configurations). The dotted lines at 1 correspond to bulk densities. Ion profiles do not spread out sufficiently to form a diffuse layer even in such a small cell until nanosecond timescales.

extending out to 10 ns (impractical in AIMD, typical in classical MD). It is only at these time scales that the ions are able to sample the spatial extent of the diffuse layer within the simulation cell. Notice that the first 2 ns chunk differs significantly from the rest, not just for the ion profiles, but also for the water profiles. This example illustrates that even if the AIMD is first equilibrated using inexpensive methods such as classical MD, the time scales of AIMD will not allow for equilibration of either the water[34,35] or the ions. This is true even if the sampled trajectory looks like it is unchanging over the (short) simulation time.

Consequently, to circumvent the diffusion time scale of ions, AIMD simulations with explicit ions typically focus on the ions in the inner (Stern) layer,[22] thereby neglecting the diffuse-layer ions. This approach works for potentials far from the potential of zero charge and at high ionic concentrations, where the Stern layer dominates. At the opposite extreme, MD simulations of neutral electrodes (at the potential of zero charge) can avoid the ion diffusion time scale by eliminating explicit ions entirely.[16,40,41] However, at intermediate potentials and concentrations, the full double layer may still be required to capture the electric properties of the interface. This requires techniques that can capture slow dynamics and rare configurations more efficiently than MD simulations, such as using enhanced sampling methods, as we discuss next.

2.4 Enhanced sampling

Time scales of dynamics of both adsorbates and the electrolyte at electrochemical interfaces can exceed the capabilities of direct MD simulations, as discussed above. Enhanced sampling techniques broadly address such time scale limits by making rare processes more probable than in an MD simulation, thereby capturing rare configurations within a fewer total number of evaluated configurations. These techniques span a wide range of complexity, starting from targeting a specific reaction with a known reaction coordinate, which could be suitable for slow adsorbate dynamics at the electrochemical interface. At the opposite extreme, all-atom enhanced sampling methods attempt to explore relevant rare processes automatically, which would be necessary for dynamics without a known reaction coordinate, such as double layer formation.

The simplest class of enhanced sampling methods follow an explicitly known reaction coordinate, *e.g.* the adsorption/desorption of a species on an electrode surface with distance from the surface serving as a reaction coordinate.[42] In such cases, MD simulations can be performed starting from several initial values of the reaction coordinate to ensure coverage of all relevant values of that coordinate. The trajectories of these MD simulations are then re-weighted to calculate the potential of mean force (PMF), the derivative of free energy with respect to reaction coordinate, at several values of the reaction coordinate. Approaches like the Blue Moon ensemble can prescribe ideal choices for the set of initial reaction coordinates such that the re-weighted PMF estimates are accurate for the desired range of reaction coordinates.[43] Most importantly, by integrating over the PMF, these calculations estimate reaction free energies including entropy.[44] In contrast, conventional MD simulations typically only estimate energy and enthalpy, requiring additional approximations for the entropy, such as the two-phase 2PT method that interpolates the entropy between two bulk phases.[45,46]

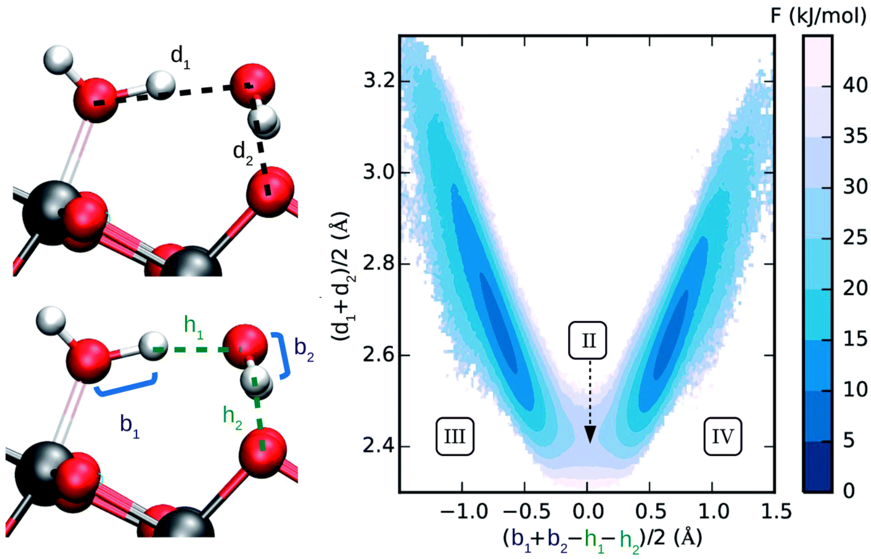

Figure 4: Enhanced sampling allows mapping the free-energy landscape of proton transfer at an aqueous TiO_2 interface as a function of collective variables based on O-O and O-H distances.[47] The predicted barrier of 25 kJ/mol would make proton transfer too rare to capture in conventional MD simulations. (Adapted from Ref. 47. Copyright 2020 Royal Society of Chemistry under (CC BY-NC 3.0).)

When the processes of interest have more complex or several reaction coordinates, starting from several initial values of the reaction coordinate can become impractical. Instead, enhanced sampling approaches such as umbrella sampling and metadynamics[48,49] apply bias potentials that make the lowest energy configurations less probable, thereby increasing the relative probability of rare configurations. The bias potentials are typically a function of collective variables that change between the low and high-energy configurations,[50] serving as generalized reaction coordinates. For example, combinations of distances between surface/water oxygen atoms and hydrogen atoms succeed as collective variables to map the free energy of proton transfer at the water-TiO_2 interface using umbrella sampling (Fig. 4).[47] A more complex case of sampling the reaction of alumina with water with metadynamics requires multiple collective variables, such as the coordination numbers of aluminum atoms by oxygen from the alumina and by those from the water.[51] See Ref. 52 for a detailed review of such enhanced sampling techniques applied to AIMD simulations of reactions at solid-liquid interfaces.

Finally, enhanced sampling techniques can also be applied beyond specific chemical reactions to capture more general processes without known reaction coordinates / collective variables,[53] such as ion diffusion and reorganization of strongly adsorbed species at electrochemical interfaces (Section 2.3). A number of general techniques have been developed to simulate slow processes ranging from diffusion and phase transformation in solids,[54,55] to biomolecular processes including protein folding.[56,57] These techniques adopt different strategies to push the simulation out of a local minimum in energy towards less-probable configurations, ranging from generalized bias potentials in the Adaptive Biasing Force method[58] to increased effective temperatures in simulated annealing, temperature-accelerated dynamics and replica-exchange MD. See Ref. 53 for a review spanning this entire range of enhanced sampling methods. The general enhanced sampling methods for complex processes without known reaction coordinates or collective variables require a much larger number of configurations ($\gg 10^6$) than practical for AIMD,[55] and have typically been restricted to classical MD. Recent developments in machine-learned force fields bridging classical MD and AIMD (Section 3.1), combined with such collective-variable-free enhanced sampling methods, will make it possible to simulate double layer formation and other dynamical electrochemical processes beyond the reach of current MD simulations.

3 Classical molecular dynamics accuracy

We next turn to the approximations for the energy and charge density employed by simulations of electrochemical interfaces, starting with classical MD simulations. At the bottom right of Figure 1, classical MD prioritizes ionic dynamics to extensively sample atomic configurations. The resulting extensive approximations to account for the electrolyte, metallic electrode, and electronic charge density (if included at all), necessitate care to accurately predict the charge density and electrostatic potential profiles of electrochemical interfaces using classical MD.

3.1 Force fields

The central approximation in classical MD is the use of force fields to describe all interatomic interactions. The accuracy of force fields depends both on the range of physical effects that they can account for, and on the data used to parameterize their empirical parameters. Most importantly, force fields for classical MD simulations of electrochemical interfaces must be simultaneously accurate for the electrode, electrolyte and electrode-electrolyte interactions.

The simplest force fields for atomistic simulations typically combine Coulomb interactions between fixed charges on each atom type, and pair potentials such as Lennard-Jones or Morse potentials to account for short-ranged repulsion and intermediate-range attractions, including dispersion interactions.[59,60] The parameters of such force fields for liquids are usually fit to reproduce the structure and thermodynamic properties of bulk liquids, based on experimental measurements or *ab initio* simulations.[61] These force fields are computationally efficient and allow simulations to access larger length and time scales, but they cannot capture variations of the interatomic interactions from bulk materials to interfaces. Additionally, for electrolytes, the parameterization of such force fields may also need to be modified when ionic concentration increases from the dilute limit towards the solubility limit.[62,63]

Polarizable force fields introduce induced dipoles in addition to fixed charges at each atom, allowing treatment of electronic polarizability.[64,65] This partially captures variations of the effective interatomic interactions with the local atomic environment, as reviewed by Ref. 66 for electrolytes. Charge equilibration (QEq) in force fields allows for even more flexibility by adjusting atomic charges based on their environment, frequently using electronegativity of atoms compared to their neighbors to determine the equilibrium charges.[67] QEq is often combined with reactive force fields that adjust short-ranged bonding and dispersion interactions based on an empirical bond order, in turn determined from the atoms surrounding each atom.[68,69] Reactive force fields have been successfully applied for reaction modeling at electrochemical interfaces,[28,29] but require careful parameterization for specific combinations of materials at the interface using extensive *ab initio* simulations to determine their large number of parameters.

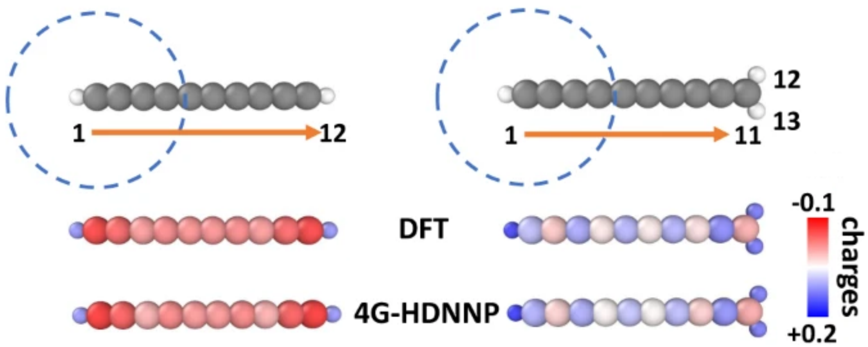

Figure 5: Recent neural network (NN) potentials predict atomic charges, including long-range rearrangements, in excellent agreement with DFT calculations.[70] This is necessary for including electrode potential effects in electrochemical MD simulations with NN potentials. (Adapted from Ref. 70. Copyright 2021 Springer Nature under (CC 4.0).)

All the above force field models employ specific functional forms for each of the physical effects that they empirically approximate. In contrast, machine-learned (ML) force fields use highly flexible functional forms that can capture virtually any form of interatomic interactions,[71] provided enough data from *ab initio* calculations.[72] In particular, neural network (NN) models are highly versatile for predicting forces and energies as a general function of the local environment of each atom.[73] Most NN force fields include the forces due to Coulomb interactions implicitly, and have been shown to predict atomic structures of electrode-electrolyte interfaces with sufficient accuracy.[74,75] However, without explicit atomic charges, such models cannot account for long range electrostatics and electrode potential effects important for electrochemistry.[74,76] Classical MD simulations for electrochemical interfaces should therefore take advantage of recent NN force-field developments that explicitly model global rearrangements of atomic charges (Figure 5) depending on the atomic environment,[70,76–80] using a generalization of the QEq method.[67] Finally, ML force fields can be learned on-the-fly during the course of AIMD simulations.[81–83] This facilitates skipping the electronic structure calculation automatically when the ML force predictions are sufficiently accurate, potentially bridging the time scales accessible by AIMD and classical MD simulations.

3.2 Fixed-potential treatment of metal electrodes

Classical MD approximations of interatomic interactions must account for the redistribution of charges over long distances by metallic electrodes. The electrode potential fixes the electron chemical potential, allowing the number of electrons at the surface to freely equilibrate as the charge of the electrode reaches its equilibrium value.[2] Fixing the charge at this equilibrium value and letting the potential fluctuate around its equilibrium value instead will yield equivalent thermodynamic averages between these two ensembles. This is the case for first-principles calculations where fixed-potential and fixed-charge calculations are equivalent for averages (but differ in fluctuations) as long as they describe a charged interface with the same equilibrium charge and potential.[84]

However, 'fixed-charge' classical MD simulations conventionally refer to fixed *atomic* charges, rather than fixed *total* charge.[86] They describe the electrode as a slab where the net surface charge is distributed among the surface atoms, and this charge stays fixed throughout the simulation. In a real metal (and in all AIMD and in *some* classical MD[85–88] calculations), the charge distribution of a metal electrode will respond automatically to make its surface equipotential. (This assumes an ideal metal with a high electronic density of states, where the electrostatic potential is screened within a fraction of atomic dimensions; we discuss finite Thomas-Fermi screening length effects in Section 3.3.) This rearrangement leads to an attraction between charges in the electrolyte and the induced charge distribution in the metal (Fig. 6(a)). Charges on a typical classical MD slab do not respond to the electrostatic

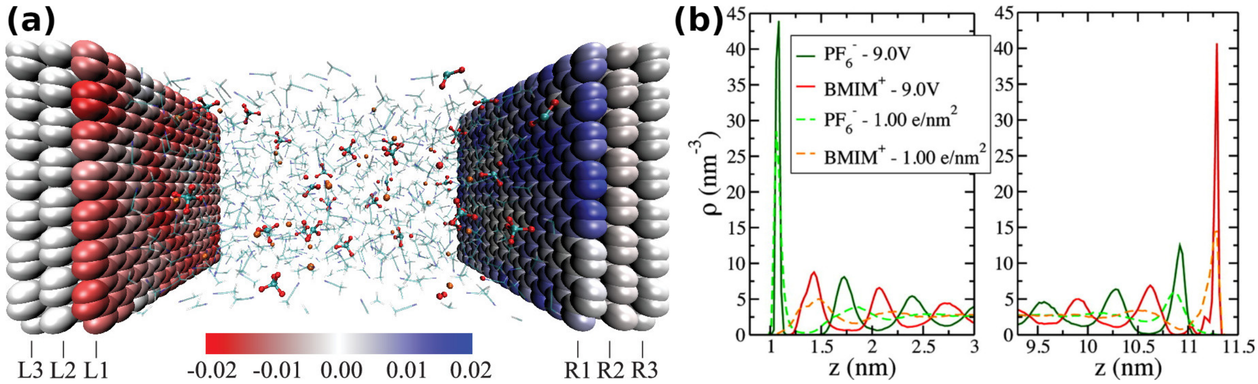

Figure 6: (a) Fixed-potential MD simulations capture localized induced-charge response of the metal electrode,[85] causing (b) an increased effective attraction of charged electrolyte species to the electrode leading to substantial differences in ion distributions next to the electrode.[86] ((a) Reprinted from [*J. Chem. Phys.* **141**, 184102 (2014)], with the permission of AIP Publishing. (b) Adapted with permission from [*J. Phys. Chem. Lett.* 2013, 4, 2, 264–268]. Copyright 2013 American Chemical Society.)

environment and miss this charge to induced-charge attraction with the electrode. Fixed-potential MD simulations capture this interaction, making them physically distinct from fixed-charge MD simulations.[85,87–90]

Simulating a metal surface in MD and correctly describing the fixed, constant potential requires specialized techniques beyond application of standard force fields with fixed pair interactions.[37,91–93] The localized dipole response of polarizable force fields (Section 3.1) may approximate the induced charge distributions of metal surfaces for large enough polarizabilities,[64] but cannot capture the complete charge rearrangement that makes a metal surface equipotential in general. The global reassignment of charge in reactive force fields[67–69] are designed to capture charge transfer between adjacent atoms in different chemical environments, but cannot reliably capture a metallic response. Similarly, the nonlocal charge transfer in recent NN force fields (Section 3.1) has so far focused on molecular and non-metallic systems,[70] and may require further development to achieve reliable treatment of the metallic response.

Initial treatment of fixed potential in MD relied on image-charge methods: the electrostatic potential near an ideally planar metallic electrode can be computed as the combined potential from all the charges in the electrolyte and their reflection (with negated charge) about the electrode plane.[94–96] This technique does not require adjustment of charges to capture the equipotential and can capture the attraction of the charged liquid species to the metal as their attraction to their own image charges. However, this only works for a single ideally flat electrode surface, and does not easily generalize to other geometries.

A more general scheme of fixed potential in MD explicitly adjusts the charges of all metal atoms in the simulation, solving a set of dense linear equations at each time step to ensure that the electrostatic potential on each metal atom equals the electrode potential.[87–89] This is more computationally demanding, requiring multiple evaluations of the long-range Coulomb interactions in reciprocal space,[97] which is the most expensive component of classical MD force fields, in addition to the dense linear solve. However, the generality of this approach allows treatment of arbitrary electrode geometries and is increasingly available in classical MD software.[85,98]

Several comparisons between fixed *constant* charge and fixed potential simulations have demonstrated that fixed charge simulations may incorrectly model the charge response.[99] Large charge localized on the surface means that fixed potential simulations can access more favorable electrode-electrolyte interactions.[85,86,100] Figure 6(b) shows that the increased effective electrode-electrolyte attraction in the fixed potential method leads to larger peaks in the electrolyte structure of an ionic liquid next to the electrode, compared to a fixed charge simulation at the same net surface charge density.[86] This difference in the ion distributions of ionic liquids next to the electrode further increases with increasing electrode potential.[85] The ion distribution differences also impact the electrochemical capacitance of the interface, causing a reduction of the characteristic double hump behavior in fixed potential calculations compared to fixed charge calculations.[100]

To examine the conditions under which the metal induced charge interactions captured by the fixed potential methods are important, Figure 7 compares fixed charge and fixed potential methods for molten NaCl next to weakly and strongly attractive walls. Specifically,

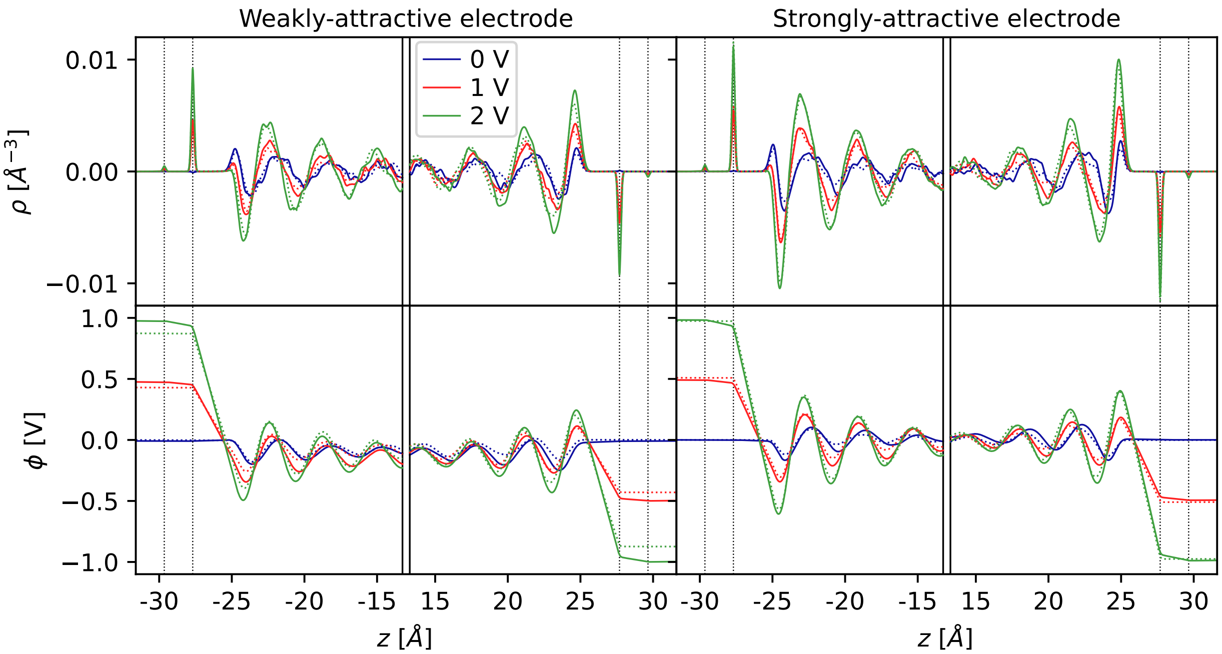

Figure 7: Comparison of charge density (top panels) and electrostatic potential (bottom panels) between fixed-potential (solid lines) and fixed-charge (dotted lines) molecular dynamics simulations of molten NaCl. The weakly-attractive electrode (left panels) shows noticeable charge density and electrostatic potential differences between the two methods because the fixed charge method misses an image charge interaction with the metal electrode. This missed interaction is less significant for a strongly-attractive electrode (right panels).

we simulate 711 ion pairs in a $25 \times 25 \times 50$ Å region between two Pt(001) electrodes using LAMMPS[39] with standard Fumi-Tosi parameters for NaCl.[101] The strongly attractive wall uses Cl parameters for the metal-ion interactions,[88] and the weakly attractive wall uses the same repulsion but scales down the attraction by a factor of 10. We perform simulations with the constant potential method first,[85] and then with the conventional fixed charge method for the same net electrode charges. Notice that the difference between the fixed charge and potential methods in Figure 7 is most significant for the weakly attractive wall, where the image charge interaction of ions with the metal is relatively more important. The differences in the potential profile and charge density are negligible for the strongly-attractive wall. Consequently, while the fixed potential method is more natural to describe a metal electrode, the more computationally efficient and widely-available fixed charge method may suffice if the wall-ion attraction is sufficiently strong. Alternatively, one could parameterize the empirical wall-ion interaction potential to effectively include the image-charge attraction.

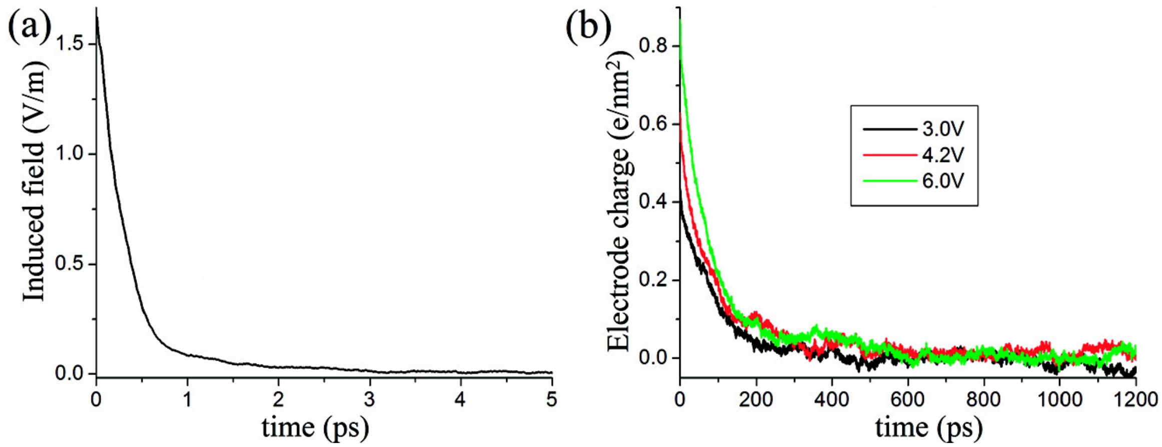

Figure 8: (a) Induced field in the electrolyte decays within picoseconds, but (b) the electrode charge equilibration on change of potential requires hundreds of picoseconds for ion diffusion, as revealed by fixed-potential molecular dynamics simulations.[102] (Adapted with permission from [*J. Phys. Chem. B* 2011, 115, 12, 3073–3084]. Copyright 2011 American Chemical Society.)

This equivalence between fixed potential and fixed charge MD with a modified wall interaction is however *limited to equilibrium properties* of the electrochemical interface. When considering fluctuations of the electrode charge,[103–105] or the dynamics of double layer formation, the differences between fixed charge and fixed potential are more fundamental.[1,86,102] The double layer typically approaches its equilibrium structure much faster in a fixed charge simulation, where the electrode always has the target charge density which sets up the electric field that drives the ion distributions to their equilibrium values. However, in a fixed potential simulation (that matches the experimental scenario), the electrolyte near the interface is initially not charged and will respond only over longer time scales of several nanoseconds.[106] At these initial times, the capacitance of the interface is low since it is determined entirely by the electronic response of the electrode. The corresponding small charge at the electrode implies a low electric field and driving force towards equilibrium ion distributions. Therefore, the rate at which ion distributions build up in the double layer are much slower in the fixed potential method (Fig. 8), and are artificially too fast in the fixed charge method. Once the double layer has formed, and electron transfer reactions are not present,[107,108] the differences between the two methods reduce to the different effective electrode-electrolyte interaction potentials as discussed above.

3.3 Electronic polarizability corrections

Fixed potential classical MD simulations discussed above capture the redistribution of charge between metal atoms in the electrode, but the charge is still located on the metal atoms. In contrast, the electron density determines the spatial extent of the charge response of electrons, and typically extends past the atom positions by (0.5 to 1) Å.[109] Not accounting for electronic polarizability therefore increases the 'gap', d, between the induced charge locations of the electrode and electrolyte by $\gtrsim 1$ Å. This gap introduces an extra series capacitance $\epsilon_0/d \lesssim 10\ \mu\text{F/cm}^2$, which is then the upper limit on the total capacitance of electrochemical interfaces predicted by classical MD simulations. Consequently, classical MD simulations that do not account for electronic polarizability grossly underestimate electrochemical capacitance,[110] especially for metal electrodes with typical experimental capacitance $\sim$ (20 to 50) $\mu\text{F/cm}^2$.

The missed contribution due to the electronic polarizability can be compensated by replacing the classical MD charge on the surface atoms with a charge density that extends beyond the plane of the electrode, towards the electrolyte.[21] The simplest version of this amounts to shifting the plane of electrode charge in classical MD towards the electrolyte, effectively reducing the gap and increasing the capacitance.[111] This is equivalent to adding a surface dipole potential (Figure 9(a)),[110,112] whose magnitude is determined empirically or from electronic DFT calculations of the electrode under an applied electric field.[113,114] More generally, the classical MD charge density can be replaced by an electron density profile calculated using DFT, thus including nonlinear changes of the electronic response with electrode potential that can affect the shape of the capacitance curves (Figure 9(b)).[21,115] Alternately, the mean electrostatic potential from classical MD of the electrolyte can be incorporated into electronic DFT of the electrode to include a degree of self-consistency in the interfacial response.[116]

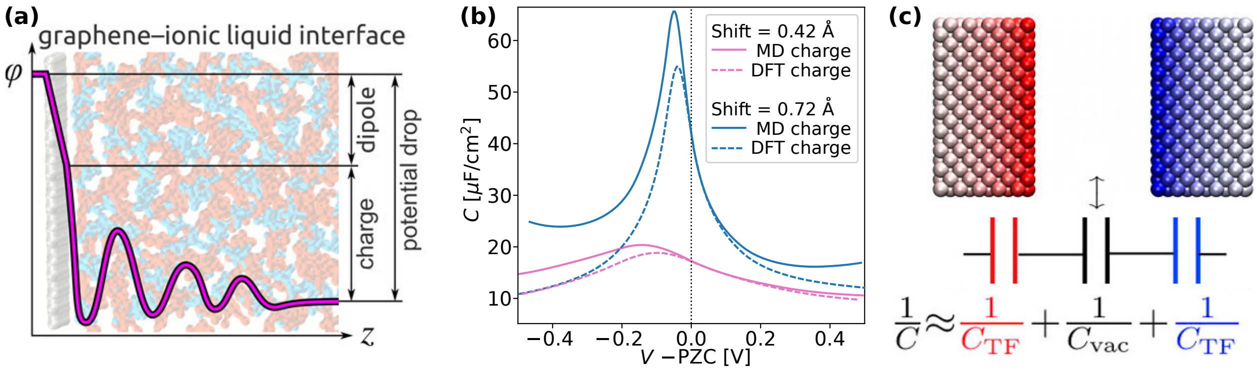

Figure 9: The underestimation of electrochemical capacitance by classical MD can be fixed by (a) a dipole correction that accounts for the electronic induced charge distribution,[114] or equivalently, (b) a shift of the electrode charge density towards the electrolyte.[21,115] (c) Additionally, a semi-classical Thomas-Fermi model can approximately incorporate electronic screening of the electrode to decrease the overall capacitance for electrodes that are not perfect conductors.[117] ((a) Adapted with permission from [*J. Phys. Chem. C* 2020, 124, 36, 19548–19555]. Copyright 2020 American Chemical Society. (b) Adapted from [*J. Chem. Phys.* **156**, 014705 (2022)], with the permission of AIP Publishing. (c) Adapted from [*J. Chem. Phys.* **153**, 174704 (2020)], with the permission of AIP Publishing.)

For electrodes that are not perfect conductors, efforts have been made to account for both the electronic polarizability of the electrode and the electrode screening. In one such approach based on the jellium model for metals, metal electrons described by a semi-classical Thomas-Fermi model are directly included in the classical MD simulation.[117] These metal electrons are assumed to extend beyond the electrode surface by half the spacing between layers. The Coulomb term of the classical MD is then modified to include electronic polarization at the Thomas-Fermi level, with a screening length dependent on the electron density of the electrode material, which effectively introduces a series capacitance at the surface of each metal electrode (Fig. 9(c)). These two steps collectively amount to moving the electronic response nearer to the liquid compared to the surface atoms for high electron-density materials like metals, but also allow for the response to move further from the liquid for low electron-density materials, e.g., in graphitic electrodes.[117]

Electronic contributions in classical MD have been included for graphitic electrodes and to a lesser extent, bare metallic electrodes.[21,116] Extending this approach to more general electrodes, especially involving functional groups, ligands or adsorbates attached to metals requires additional care. In such cases, the effective location of the induced charge density can move from the surface of the metal to the tip of the surface-attached species.[118] Such effects are highly sensitive to the nature of bonding of the species at the surface and are challenging to treat within classical MD, requiring an explicit electronic structure treatment.

4 Electronic structure accuracy

Electronic structure methods are necessary to capture changes in chemical bonding for reaction modeling and to fully account for electronic polarization effects at the interface. In principle, an electronic structure method could accurately describe the metallic electrode, reacting species, solvent, and electrolyte on the same footing. Such electronic structure methods could be used to evaluate configurations within an (AI)MD simulation, or specific adsorbate configurations and reaction paths as discussed later in Section 5.

Kohn-Sham density-functional theory (DFT) is the most commonly employed electronic structure method and has been highly successful at identifying reaction sites, structures, and reaction mechanisms in catalysis.[119–123] Briefly, DFT solves the Schrödinger equation for independent single electrons in an effective potential that approximately captures electron-electron interactions based on the electron density. Energy contributions beyond the average Coulomb interaction of electrons are captured by the exchange-correlation functional, which is typically treated semi-locally as a function of only the local electron density and its gradients. (See Ref. 124 for a detailed introduction.) However, the approximation of the electron-electron interactions within DFT, which makes it computationally practicable, can introduce significant errors in *ab initio* electrochemical simulations. DFT errors at the electrode surface include inaccurate adsorbate binding energies on metal surfaces, regardless of exchange-correlation functional,[5,125–128] interfacial band alignment,[14,129] and surface formation energies of oxides.[130] Similarly, for the electrolyte, DFT underestimates the band gap of water, overestimating its polarizability,[131] and hence its dielectric constant.[132–134] Additionally, DFT errors in dispersion and many-body interactions in liquid water lead to errors in liquid structure,[135] while self-interaction errors limit accuracy of binding energies between ions and solvent in aqueous electrolytes,[136] and between ion pairs in ionic liquids.[137]

The inaccuracy of DFT has prompted empirical approaches to predict catalytic activity by correlating electronic structure descriptors from DFT,[138] such as d-band positions,[139,140] with experimental activity. However, these approaches do not improve on the accuracy of DFT in modeling electrochemical interfaces. We focus first on empirical corrections to improve DFT energy predictions. We then discuss *ab initio* methods beyond DFT that can simulate electrochemical interfaces with higher fidelity.

4.1 Empirical corrections to DFT predictions

Empirical approaches use data from experiments or higher-level computational methods to compensate for the limited accuracy of DFT electronic structure predictions for specific properties of a narrow range of systems.

4.1.1 Experiment-based corrections

Inaccuracies in gas phase energies of molecules frequently dominate adsorption energy errors in semi-local DFT functionals. Rectifying the gas-phase energies of molecules involved in adsorption energy calculations can substantially reduce overall errors. For example, empirical gas-phase energy corrections derived from experimental formation energies reduce the average error in onset potential of CO_2 to CO reduction on 7 metal surfaces from 0.20 to 0.06 V.[141] However, solvent-binding and electrification effects can also impact adsorption energies (and hence onset potentials) by 0.1 – 0.2 eV,[142] necessitating treatment beyond gas-phase corrections for systematic modeling of electrochemical reactions.

Beyond gas-phase corrections, empirical corrections to DFT modeling of molecules adsorbed on surfaces may adapt the DFT exchange-correlation for a specific reaction or class of systems. For example, specific reaction parameter (SRP) DFT linearly combines different exchange-correlation functionals to cancel DFT errors optimally, originally demonstrated for dissociative chemisorption of H_2 on metal surfaces.[143] The linear combination coefficients are fit to experimental sticking curves from supersonic beam experiments and are typically dependent on the reaction and specific metal surface.[144–146] (See Ref. 147 for a review of SRP methods.) Extending such techniques from surfaces in vacuum to electrochemical interfaces will require comparably sensitive experimental probes of binding energies and reaction rates. A further challenge in linear combinations to cancel DFT errors in surface adsorption and reactions is that the optimum combination may depend on the nature of the binding interaction. Adapting the linear combination to transition between different parameters for covalent and vdW binding, for example, better fits a wider range of systems than a fixed linear combination of DFT methods.[126] These methods are currently optimized for adsorption of a single species, and hold promise as a tool for simplified calculations of electrochemical environments (e.g., without co-adsorption of multiple species and solvents).

4.1.2 Delta-learning to beyond-DFT methods

Empirical corrections to DFT for more complex electrochemical interface structures are challenging to achieve based on limited experimental measurements alone. Instead, *ab initio* simulations beyond DFT can resolve many of the accuracy limitations of DFT as discussed next in Section 4.2, and can be performed more readily for a specific atomic configuration of the interface. While beyond-DFT approaches can also be used directly for predicting electrochemical processes, albeit with high computational costs, they can also be useful to generate data for empirical models that can make rapid predictions for a wider class of systems.

At the simplest limit of such approaches, relatively few beyond-DFT calculations can be used to fit a linear extrapolation of a specific property such as binding energy from DFT to a higher-level electronic structure method.[148] Machine-learning (ML) methods can capture more complex trends and increase the generality of such predictions. ML methods can be used to bypass electronic structure calculations, both as force fields for specific systems (Section 3) and for property predictions across classes of systems.[149] However, this typically requires a very large number ($10^3 - 10^4$) of calculations that is achievable at the DFT level, but more challenging for beyond-DFT methods.

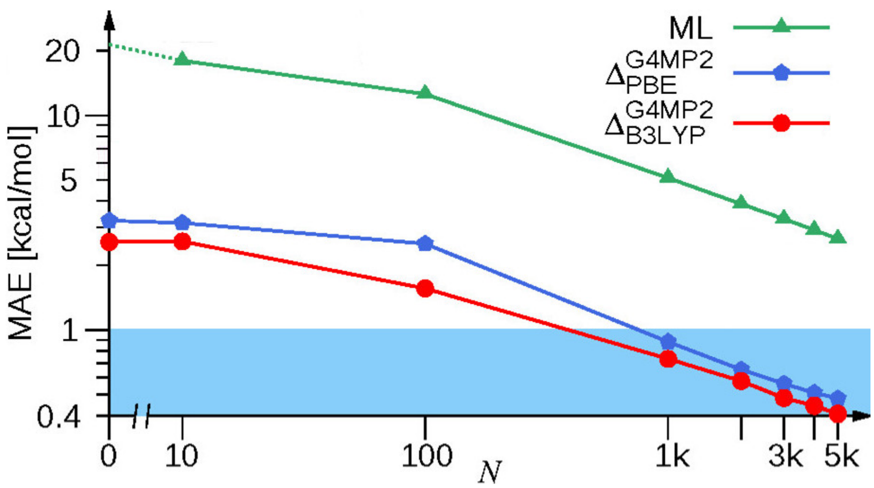

Figure 10: The mean absolute error (MAE) in atomization energies of molecules from machine learned (ML) models compared to a beyond-DFT method (G4MP2) as a function of number of molecules, N, in the training set reduces drastically when the model is trained to the difference $\Delta^{\mathrm{DFT}}_{\mathrm{G4MP2}}$ between DFT (either PBE or B3LYP) and the beyond-DFT method.[150] Such Δ-learning approaches allow beyond-DFT accuracy at DFT cost with far fewer expensive beyond-DFT calculations. (Adapted with permission from [*J. Chem. Theory Comput.* 2015, 11, 5, 2087–2096]. Copyright 2015 American Chemical Society.)

Delta learning, a general approach to learn the difference between a low and high-level prediction, rather than learning the higher level prediction directly, provides a pathway to significantly reduce the necessary number of beyond-DFT calculations. In this approach, DFT is applied to a set of systems, a higher-level method is applied to a subset of those systems, and an ML model is trained to the difference between the two methods, additionally allowing properties from the lower-level DFT calculation as inputs to the model. For example, an ML model using the DFT electron density can learn the difference in predicted energies between DFT and quantum chemical methods (Section 4.2.3) for a wide range of molecular geometries,[151] with far fewer calculations in the training set compared to ML models trained to the higher-level method alone (Figure 10).[150] Similarly, delta-learning between DFT and the random-phase approximation (Section 4.2.2) shows promising results for solid-state systems[152] and molecule adsorption on solid surfaces,[153] requiring very few (tens) of RPA calculations. Leveraging such approaches for electrochemical reaction modeling require accurate, beyond-DFT electronic structure methods that are tractable for modeling electrochemical interfaces, as we discuss next.

4.2 Beyond-DFT methods

Empirical corrections to DFT properties can improve prediction accuracy without increasing computational cost, but their utility is restricted to systems similar to those used to train the model. Electrochemical interfaces for even a single reaction can vary substantially in the electrode composition and surface structure, electrolyte species, surface coverage, and co-adsorbates. Capturing this variety in data sets for empirical correction approaches is challenging. Consequently, improving the electronic structure method itself would facilitate detailed exploration of electrochemical processes more generally. In particular, an improved electronic structure method would need to address: missing long-range correlations between electrons that include dispersion interactions, unphysical self-interaction between electrons, and a poor description of strong correlation among electrons, as discussed below. Here, we outline the possible approaches starting with improved DFT functionals, followed by perturbative treatment of many-body effects missed by DFT, and fully many-body approaches. We end with a discussion of quantum embedding approaches as a strategy for balancing accuracy and computational cost.

4.2.1 DFT methods beyond semi-local functionals

We first discuss approaches to mitigate the above issues within the formalism of density functional theory. For dispersion (van der Waals) interactions, approaches to correct for the missed long-range correlations range from empirical pair-potential corrections,[154–156] to non-local functionals that approximate the local electronic polarizability using density-functional techniques.[157,158] See Ref. 159 for a detailed review of van der Waals functionals in DFT. Recent electronic vdW functionals capture dispersion interactions more generally across material systems than empirical approaches, and compare better with experimental binding energies than semi-local DFT. Figure 11(a) shows that a nonlocal vdW correction (vdW-DF[157]) significantly improves the underestimated binding energy of graphite by local (LDA) and semi-local (PBE) DFT. However, the vdW density functional results are still inaccurate compared to experiment.[160] This is observed more generally in other systems and with other vdW functionals. For instance, the structure of liquid water predicted by DFT is improved,[161,162] but not fully corrected by vdW density functionals due to missing beyond-two-body dispersion interactions.[135,163] Consequently, approaches beyond both empirical corrections and vdW density functionals are necessary for a more universally accurate treatment of long-range correlations.

Improved electronic structure methods also need to correct the self-interaction error in DFT. Specifically, the mean-field Hartree term (Coulomb interaction computed on the electron density) in DFT includes a spurious repulsion of each electron by itself, which is only partially cancelled by semi-local exchange-correlation functionals. This spurious repulsion leads to the general underestimation of DFT band gaps. For adsorbates on metal surfaces, self-interaction errors lead to incorrect energy level alignment between the molecules and the metal surface.[5,164] This can lead to significant errors in the charge state and binding energy of adsorbates,[6,125,128] limiting the accuracy of semi-local DFT predictions for electrochemical reactions. Direct subtraction of self-interaction errors for each single-electron wavefunction improves electronic structure in certain cases,[165] but depends on the choice of orbitals (not invariant under unitary transformations of occupied orbitals),[166] and has so far been limited to molecules and finite clusters of atoms.

The most computationally-efficient semi-empirical approach to partially correct self-interaction errors is DFT+U.[167,168] This technique adds energy corrections for electronic states localized to each atom based on an empirical parameter U for each atomic species with localized orbitals (such as d-orbitals). See Ref. 169 for a detailed overview of DFT+U methods. DFT+U is useful as a quick fix for d-electron inaccuracies in electronic structure and energetics of transition metals and compounds. However, it performs less reliably when moving from bulk to surface properties, such as surface formation energies, because of varying electronic environments for the same atom type.[170] Most importantly, DFT+U introduces non-systematic errors in adsorption energies, activation barriers and reaction energies on transition-metal containing catalysts,[171] making it unsuitable as a general-purpose technique for first-principles electrochemistry.

Currently, hybrid functionals, which include a fraction of the exact exchange energy, calculated from the electron wavefunctions rather than approximately from the electron density, are the most widely applied approach to mitigate self-interaction errors in semi-local DFT.[172] Exact exchange cancels out the self interaction in the Hartree term exactly for one-electron systems, but it overcorrects many-electron systems because it does not account for screening of the exchange interaction by other electrons. Hybrid functionals address this issue by using only a fraction of exact exchange,[173,174] and in screened-exchange functionals, by additionally using a short-ranged Coulomb operator in the exact exchange calculation.[175] The partial cancellation of self-interaction errors in hybrid functionals leads to significant improvements in both adsorption energies and reaction barriers for molecules on surfaces.[164]

In principle, the exchange fraction and screening length should depend on the dielectric response of the material. General-purpose hybrid functionals use empirical values for these parameters that work across a class of materials and properties of interest e.g., reaction barriers in molecules or band gaps of solids, and have been highly successful for those materials and properties. A non-empirical approach to hybrid functionals by setting exchange fraction based on the dielectric constant works well for band gaps of semiconductors.[176,177] In this regard, the appropriate exchange fraction for metals with strong screening of the exchange interaction is zero, and indeed hybrid functionals generally perform worse for metals than semi-local DFT.[178,179] This poses a challenge for rigorously modeling electrochemical interfaces that combine metals,[178,179] adsorbed molecules at the surface,[180,181] and fluids with a large band gap in a single calculation, each of which require a different exchange fraction for accurate treatment using a hybrid functional.[182]

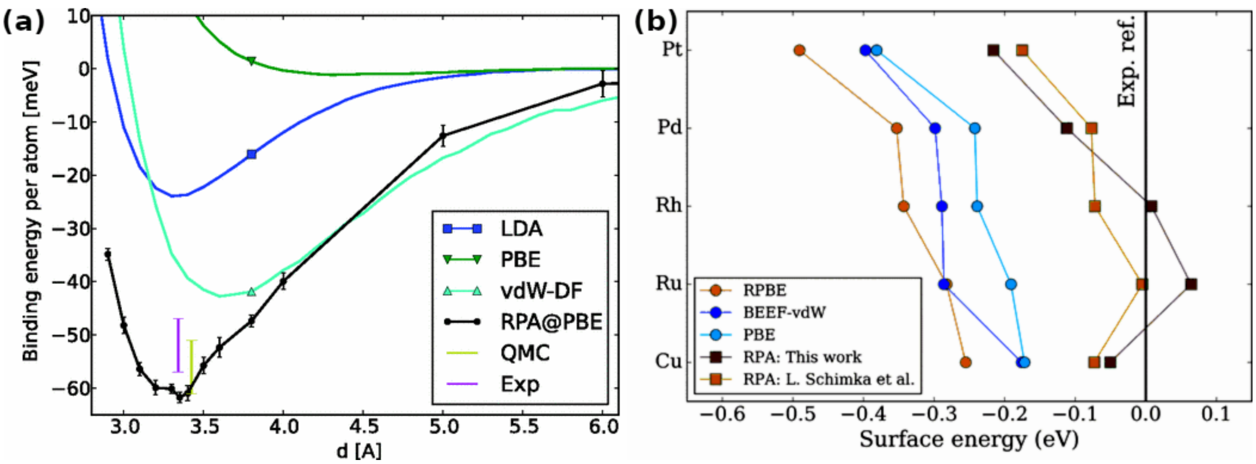

Figure 11: (a) Semi-local and nonlocal vdW-DF density functionals underestimate binding energy of graphite, while RPA agrees closely with QMC simulations and experiment.[160] (b) DFT also underestimates surface energies of metals, while RPA agrees with experiment.[183] ((a) Adapted figure with permission from [*Phys. Rev. B* **87**, 075111 (2013)]. Copyright 2013 by the American Physical Society. (b) Adapted with permission from [*J. Phys. Chem. C* 2018, 122, 8, 4381–4390]. Copyright 2018 American Chemical Society.)

4.2.2 Many-body perturbation theory

Accurate treatment of electronic structure across a large range of electronic environments, *e.g.*, metal to fluid in an electrochemical interface, generally requires many-body techniques beyond DFT that explicitly account for electronic screening. Missing long-range correlations and self-interaction errors in DFT discussed above all stem from the use of a single non-interacting electronic wavefunction (Slater determinant of one-electron orbitals). Many-body pertubation theory approaches start from this wavefunction and introduce electron correlation effects perturbatively. The most common approaches to explicitly calculate correlations are based on the electron Greens function $G(r, r', t' - t)$, which describes the expectation of finding an electron at position r' and time t', after introducing one at r and earlier time t. The GW method approximates G starting from the corresponding non-interacting Greens function G_0 of DFT, and the (time/frequency-dependent) screened Coulomb potential $W(r, r', t' - t)$ computed explicitly from DFT. GW leads to more accurate predictions of electronic band structures that account for many-body electron effects (correlations).[184] The corresponding calculation of the total energy of the electronic system corresponds to the random-phase approximation (RPA) method. See Ref. 185 for a review of the RPA approach to the electronic correlation energy.

Notably, the scaling and computational cost of GW and RPA are between that of DFT and the potentially more accurate quantum-chemistry methods discussed in the next section, and they are routinely applied to extended systems, including metals and metal surfaces. These techniques explicitly account for the screening of the Coulomb and exchange interactions by the electrons of the system, and are therefore applicable to electrochemical interfaces combining metals, molecules and fluids. In particular, they predict the level alignment between molecules / molecular liquids and metals accurately,[3,4] which is critical for capturing the correct charge states of reacting species at an electrochemical interface within RPA total energy calculations.

RPA directly includes long-range correlations and thereby captures dispersion (vdW) interactions without additional corrections across diverse chemical environments. Figure 11(a) shows that RPA predicts the binding energy and distance of graphite in excellent agreement with experiment and quantum Monte Carlo simulations, in contrast to vdW DFT functionals that underestimate the binding strength.[160] It also predicts the formation energy of metal surfaces – important for describing energetics at an electrochemical interface – much more accurately compared to experiment than any semi-local or vdW DFT functional (Figure 11(b)).[183] However, traditional RPA without an exchange-correlation contribution within the screened Coulomb potential W can be less accurate for covalent bonds than hybrid functionals.[160] Consequently, applications to electrocatalysis should employ recently modified RPA methods that include a renormalized DFT exchange-correlation screening kernel, which makes RPA more accurate for both covalent and vdW interactions.[186]

4.2.3 Wavefunction / quantum chemical methods

An alternative to capturing many-body effects perturbatively is to directly work with many-body electronic wavefunctions. Quantum chemical / wavefunction methods typically solve for the many-body electronic wavefunction as a linear combination of several non-interacting wavefunctions. The most direct approach of considering all such linear combinations – the full configuration-interaction (FCI) approach – scales exponentially with the number of electrons and is practical only for atoms and very small molecules. In practice, quantum chemical methods restrict the choice of non-interacting wavefunctions from this exponentially-scaling set. For example, coupled-cluster techniques typically account for combinations of single and double excitations relative to the ground-state wavefunction. See Ref. 187 for an introduction to quantum chemical methods.

For molecular reactions, these coupled-cluster techniques are systematically improvable and provide the best accuracy.[187,188] Quantum chemistry methods implicitly account for electron correlations, including long-range vdW interactions, and therefore would be desirable for accurately describing molecules on surfaces for electrochemistry. However, these methods are restricted to finite molecular geometries due to their computational cost. Application to heterogeneous catalysis typically involves replacement of solid surfaces by small atom-cluster surface models.[189] Alternately, a cluster of atoms treated with quantum chemistry may be embedded within techniques suitable for solids, as discussed below in Section 4.2.5.

4.2.4 Quantum Monte Carlo simulations

An alternative class of techniques to account for many-body electronic effects are quantum Monte Carlo (QMC) techniques, which use stochastic methods to solve the many-body Schrodinger equation and find the ground state energy of an electronic system.[190] The domain of stochastic exploration in QMC may range from real space in diffusion Monte

Carlo (DMC) to the space of non-interacting wavefunctions (Slater determinants) in full configuration-interaction QMC (FCIQMC) methods. FCIQMC operates in a similar space as quantum chemical methods, and is most developed for calculations of molecules and, to a lesser extent, non-metallic solids.[191] Out of the family of QMC methods, diffusion Monte Carlo (DMC) is currently most suited to periodic calculations of electrochemical systems. It has more favorable scaling (at worst, N^4 in practice[192]) with system size than quantum chemical methods. See Ref. 193 for a review of QMC methods.

Diffusion Monte Carlo (DMC) captures dispersion interactions, describes metals correctly, and has been used to describe adsorption energies as well as reaction barriers for molecules on transition metal surfaces.[194–199] DMC can be very accurate, with the potential to have errors smaller than 'chemical accuracy' of 1 kcal/mol. Recent advances to automate convergence of statistical errors,[192,200] and to mitigate finite size errors that are particularly important for metallic systems,[201,202] bring DMC closer to being a widespread option for chemistry at metallic surfaces. Combined with the development of solvation models compatible with quantum Monte Carlo methods,[203] including techniques to deal with statistical errors in the electron density[204] and achieve self-consistent solvation by electrolytes,[205] DMC is now within reach for electrochemical simulations.

4.2.5 Quantum embedding methods

A remaining hurdle in widespread application of any of the above beyond-DFT methods for electrochemistry is the significantly higher computational cost compared to DFT. This could be mitigated by using quantum embedding techniques – applying higher-level electronic structure to only a portion of the system, along with lower-level methods for the remainder of the system.[206] Embedding is particularly useful for simulating molecules adsorbed on metal surfaces, with quantum chemical methods applied to the molecule and a cluster of metal atoms closest to it, and methods more amenable to periodic systems such as DFT applied to the metal surface slab.[207] These techniques typically incorporate the potential from the lower-level DFT method into the localized quantum chemical simulation, and show great promise for circumventing DFT errors in adsorbed molecules such as for the prototypical example of CO on Cu(111).[208]

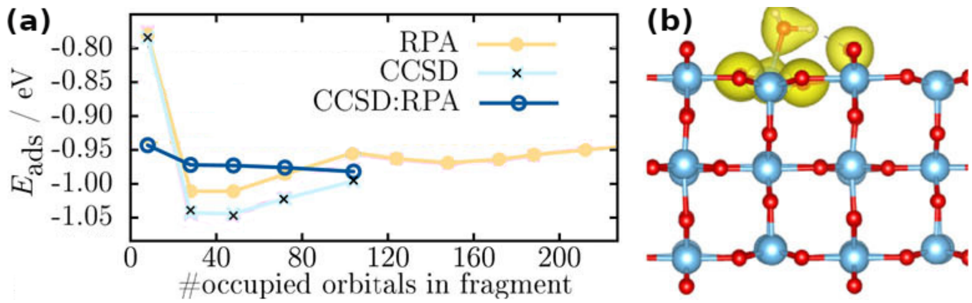

Figure 12: (a) Embedding coupled-cluster singles and doubles (CCSD) within random phase approximation (RPA) calculations results in better convergence with size of fragment, compared to equivalent embedding within DFT. Results shown here for the adsorption energy of water on a TiO_2(110) surface, with (b) showing the electron density from the occupied orbitals of the fragment treated using CCSD.[209] (Adapted from [*J. Chem. Phys.* **154**, 011101 (2021)], with the permission of AIP Publishing.)

Embedding techniques require care to ensure convergence with respect to fragment size: the size of the subsystem treated at the higher level of theory. Recent advances on several fronts show promise for maintaining accurate calculations with smaller fragments. First, the interactions between the two levels of theory can be extended beyond traditional density-functional embedding (i.e., using the electron potential) to Greens function- or density matrix-based embedding: see Ref. 210 for a detailed comparative review of these embedding formalisms. Next, improving the treatment of correlations in the lower-level method can improve the matching between different levels of methods and reduce the needed fragment size, as demonstrated for embedding coupled cluster theory within RPA for water on a titanium dioxide surface (Figure 12).[209] Finally, embedding techniques have also been demonstrated for QMC as the higher-level method, including DMC in DFT to allow treatment of larger fragments than quantum chemical methods,[211] and FCIQMC in DFT to treat higher-level correlations than coupled cluster techniques.[212]

The ability of quantum embedding techniques to combine different approaches for portions of the system makes them promising for electrochemical calculations that bring together metals, molecules and liquids with vastly different electronic structure. Further work is now necessary to test embedded methods for charged electrochemical interfaces, including electrolyte solvation, to make them widely applicable to computational electrochemistry.

5 Single configurations and their ensembles

In the previous sections, we discussed techniques of increasing accuracy along the electron axis of Figure 1 from classical MD to beyond-DFT electronic structure. The corresponding increase in computational cost typically makes dynamics intractable and necessitates a corresponding move to the left along the atom axis: towards single configurations and ensembles of few static configurations.

In this final section, we discuss the challenges inherent in approximating electrochemical interfaces by single or few structures. Specifically, selection of surface structures for adsorbates becomes increasingly important when evaluating few atomic configurations. Note that this consideration could be important for strongly-bound species at the surface even in MD simulations, since the structure of such species may not equilibrate at MD-accessible time scales. Beyond the surface-adsorbed species, weakly-interacting solvent and electrolyte interact with the surface and must be included explicitly in the simulation, implicitly using a solvation model, or a combination of such approaches. Finally, we discuss the effect of the electrochemical potential on predictions from such calculations with single / few configurations.

5.1 Surface coverage of bound species

We first discuss sampling atomic configurations for the electrode surface and its strongly-bound adsorbates that adopt one or more well-defined structures (*i.e.,* not a continuous ensemble that necessitates dynamics). However, the coverage and site preference of adsorbed species routinely change with electrochemical conditions including electrode potential and electrolyte composition. Further, the structure of the surface itself may change by reconstructions, oxidation and dissolution depending on electrochemical conditions. Consequently, selection of surface structures requires techniques to generate candidates and identify the lowest-energy configurations as a function of conditions.

First-principles simulations of electrochemical reactions frequently employ knowledge-based methods, starting from structures known from experiment and analogs to those structures. For single crystal electrodes, heuristics coupled with *ab initio* methods with limited numbers of atoms may be sufficient to create initial structures.[119] However, ensembles of structures generated in this way may be biased towards extreme coverage and simple structures, because they are typically generated with simulation size as the primary concern. Additionally, evaluation of a single structure implicitly assumes that the configurational entropy does not significantly contribute to the surface free energy.[213] Overall, heuristic approaches can be successful for systems with extensive prior experimental and computational experience, but can be biased and essentially an uncontrolled extrapolation when applying it to previously unexplored systems.

Data-driven and simulation-based approaches can provide a more systematic pathway to identifying candidate structures. Such approaches have been developed recently for neutral and unsolvated catalyst surfaces, and could be applied for electrochemical applications. Data-driven approaches to structure generation are essentially a systematic big-data limit of heuristic approaches: they use extensive databases of structures in previously studied systems to train models to generate candidate structures for new systems. While databases of structures have been well-established for solids and molecules,[214–216] the increased complexity and degrees of freedom make this much more challenging for surfaces and adsorbates. Recent databases of surface reactions for catalysis containing adsorption and reaction energies from DFT calculations,[217] and surface adsorption with both DFT and beyond-DFT methods,[183] aim to bridge this gap for surface properties. Extending coverage of such databases to additionally include electrochemical conditions of solvation and electrode potential will be vital to apply machine learning and data-mining for reliably proposing candidate surface structures for electrochemistry.

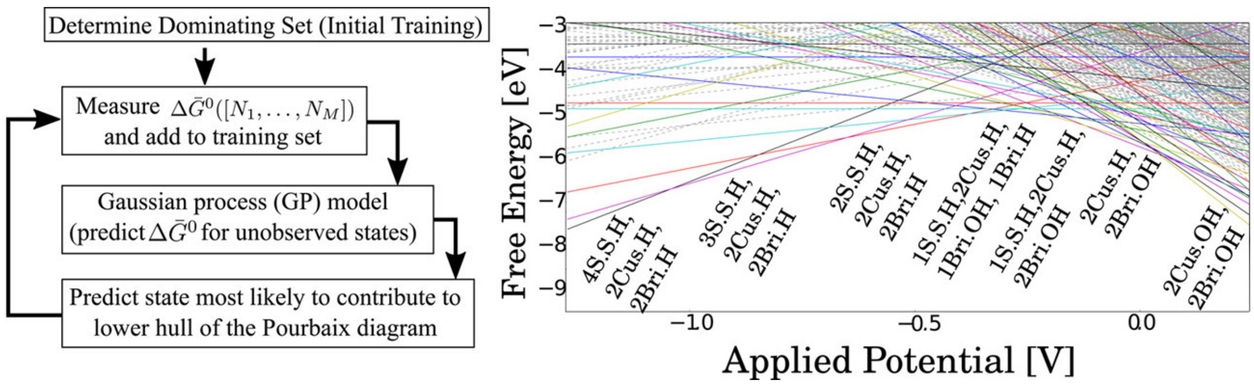

Figure 13: Determination of stable surface structures of IrO_2 as a function of electrochemical potential,[218] combining heuristics to generate structures, with *ab initio* methods and Gaussian process approximate models to evaluate energies of structures. The algorithm (left panel) captures a large number of surface structures, as depicted in the Pourbaix diagram (right panel). (Adapted with permission from [*J. Phys. Chem. Lett.* 2016, 7, 19, 3931–3935]. Copyright 2016 American Chemical Society.)

In addition to data-driven techniques that directly target structures, simulation-based approaches involve performing global searches for the minima of an energy function. The global search algorithms include Monte Carlo and evolutionary algorithms,[219] while the energy functions could be obtained directly from electronic structure methods or a range of approximations trained to such data. In the extreme limit of directly evaluating energies using first-principles methods, the number of evaluated structures during the search is typically limited to a few thousands.[220,221] This computationally-expensive direct approach has been applied to surface structures in limited contexts, such as oxidation of metal surfaces[220] and segregation of metals in alloy surfaces.[221]

More commonly, surface structure searches are performed using approximate models fit to first-principles data. Early surface structure studies employed cluster expansion methods to approximate interactions between adsorbates, and performed Monte Carlo simulations to predict coverage of adsorbates at different conditions,[222] including at electrochemical interfaces as a function of electrode potential.[223] Cluster expansions and more recent lattice-based machine-learning models[224] work best for identifying structures that involve occupation of specific adsorption sites with different coverages, without significant additional degrees of freedom. For more complex surface structures, machine-learned (ML) force fields trained to *ab initio* data (Section 3.1) can be used to accelerate the structure search.[225–227]

Figure 13 showcases a combination of above approaches to predict stable electrochemical interface structures as a function of potential.[218] Specifically, heuristics generate initial candidate structures and new structures for energy evaluation using *ab initio* methods. The lowest energy structures are used in determining new structures for evaluation, and Gaussian Process ML models trained to the *ab initio* data are used to rapidly evaluate larger numbers of structures than is practical with first-principles methods alone.[218]

5.2 Electrolyte configurations and solvation

The problem of sampling atomic configurations is not limited to the electrode surface and adsorbates (discussed above in Section 5.1), and is in fact a key challenge in accounting for solvation by the electrolyte. However, the considerations for configuration sampling differ considerably for the solvent, electrolyte, and other weakly bound species that are not limited to the surface of the electrode, and are not expected to be restricted to few well-defined structures. Importantly, it is not straightforward to avoid the problem of configuration sampling by resorting to AIMD simulations because of the time scale issues discussed in Section 2.3. Consequently, treatment of electrolyte solvation in first-principles calculations (without dynamics) falls into two categories: microsolvation, where few solvent / electrolyte configurations are included explicitly in the *ab initio* calculation, and continuum methods that directly approximate the statistically-averaged solvation effects.

Microsolvation includes solvent and electrolyte atoms directly within first-principles calculations of electrochemical interfaces, and therefore naturally describe electronic interactions between the electrolyte and the electrode. For electrodes in aqueous electrolyte, electronic interactions become increasingly important with increasing binding energy between the electrode and water.[10,41,228] The increased binding strongly affects the electrostatic potential in the electrochemical interface, leading to a difference, $\Delta\Phi$, between the potential of zero charge (PZC) of the solvated electrode and its vacuum surface counterpart, the work function.[229] Figure 14 illustrates the correlation between $\Delta\Phi$ and the adsorption energy of water, calculated from AIMD simulations. Here, *sp*-metals have the weakest water binding and the smallest value of $\Delta\Phi$, while *d*-metals have the strongest water binding and the largest value of $\Delta\Phi$. When the potential is away from the PZC, the interfacial electric field also changes the electrode-electrolyte interaction, arising from changes in orientation and polarizartion of the solvent molecules and ions in the electrolyte.

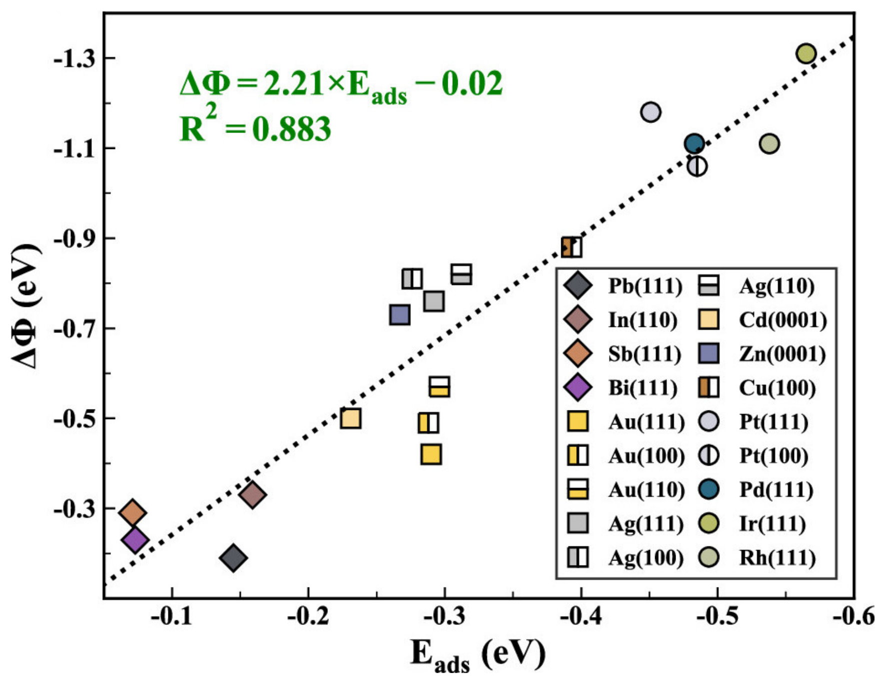

Figure 14: The difference between the PZC and work function ($\Delta\Phi$) from experiment as a function of the adsorption energy for water on metal surfaces calculated with AIMD. Surfaces include sp (diamonds), sd (squares), d (circles) metals. (Adapted with permission from *J. Phys. Chem. Lett.* 2021, 12, 30, 7299–7304]. Copyright 2021 American Chemical Society.)

While microsolvation naturally accounts for such interfacial interactions in principle, a major challenge is that the electrode potential depends on the statistically-averaged electrostatic potential and is not well-defined from a single electrolyte configuration. Averaging over several solvent configurations may partially mitigate this issue, but requires selection of specific configurations.[230,231] This is more challenging in general than for the strongly-adsorbed adsorbates discussed previously because liquid electrolytes adopt a continuously varying set of structures, and are not limited to a few local minima in energy. Often, microsolvation approaches adopt specific prescriptions for creating solvent structures for consistency,[232] but must be checked to ensure that an ensemble of such structures reproduce the bulk liquid environment correctly. For molecules in bulk solvent, quasi-chemical theory provides connections between microsolvation results and the thermodynamic ensemble average.[233] Analogously, 2D lattices of solvent molecules can be grafted onto an electrode surface to generate static interfacial solvent structures that resemble those in AIMD simulations.[234] However, the limited number of configurations and their evaluation at zero temperature (at the local energy minima) typically lead to overstructured solvent in microsolvation, compared to dynamics.[234]

At the opposite extreme, continuum solvation methods approximate the statistically-averaged interaction of the solvent and electrolyte with the electrode surface.[2] This eliminates the configuration sampling problem of microsolvation and is a good approximation for the bulk electrolyte as well as for electrolytes interacting weakly with an electrode (such as hydrophobic surfaces with aqueous electrolytes). Most continuum solvation models describe the solvent as a dielectric medium, and the effect of the electrolyte through dielectric screening. They thereby capture the dominant electrostatic interaction of the electrolyte with the charged / polarizable species at the electrode surface. However, the continuum models do not account for electronic interactions between the electrode and electrolyte, or for strong interfacial modifications of electrolyte properties (including chemisorbed solvent molecules), which affect charge distributions and adsorption energetics at strongly-interacting electrode-electrolyte interfaces.

Additionally, continuum solvation models require empirical parameterization of the solvent cavity: the boundary between the continuum and the explicit solute and surface atoms in the simulation. These parameters are typically fit to solvation free energies of molecules and ions, and require modifications for accurate prediction of interfacial properties, *e.g.*, electrochemical capacitance.[235] More advanced solvation models reduce the empiricism of cavity determination by incorporating atomic-scale distributions of the liquid with, for example, joint density-functional theory (JDFT)[236–240] or the reduced interaction-site models (RISM).[241–244] However these approaches still cannot accurately capture strong electrode-electrolyte interactions. See Refs. 2 and 17 for detailed reviews of the hierarchy of approximations, parameterization strategies and physical effects included in different classes of solvation models.

In summary, microsolvation captures local electronic structure effects at the interface, but presents challenges for statistical sampling of weakly bound solvent molecules. In contrast, continuum models directly capture the statistical average interaction of the electrolyte, but miss strong electronic structure effects at the interface. A common proposition to address these limitations is a combination of microsolvation for the first solvation shell and continuum models for the bulk liquid / electrolyte beyond it. Such hybrid methods are commonplace in homogeneous solvent-phase reaction modeling,[245,246] and are of increasing interest in electrochemical simulations.[247] However, such hybrid calculations require care to ensure that the explicit layer is sufficiently strongly bound so as to not require dynamics. It is therefore not straightforward to systematically converge these approaches with number of explicit solvent molecules, as the dynamics issues of microsolvation become more important with the addition of weakly-bound molecules. Further, simple parameterizations of solvation model cavities may spuriously introduce continuum response within gaps in the explicit solvent, necessitating nonlocal parameterizations that ensure that the continuum response is only introduced where entire solvent molecules may fit.[205,248,249] Finally, combining MD of explicit solvent molecules with continuum solvation presents additional challenges in closely matching the explicit and implicit solvation, analogous to force-field matching in hybrid quantum mechanics / molecular mechanics QM/MM MD simulations.[250,251] Similarly, mismatch in the electrostatic response at the explicit - implicit interface will require care when evaluating the charge distribution, electrostatic potential and capacitance of electrochemical interfaces.

5.3 Electrode potential effects

With candidate structures identified (Section 5.1) and simulated with solvation effects included (Section 5.2), the final task is mapping the properties of these specific structures and their thermodynamic average as a function of electrode potential. In principle, with recent techniques such as grand-canonical DFT,[84] it is possible to directly compute the grand free energy of the electrochemical interface for several electrode potentials. However, this involves additional computational cost from repeated electronic structure calculations for several potentials at each surface configuration. Here, we discuss approaches to approximate the electrode-potential dependence of the grand free energy and derived properties of surface configurations, and when such simplifications are appropriate.

The grand free energy is most commonly approximated to be a linear function of the electrode potential within the computational hydrogen electrode (CHE) approach often used in electrochemical reaction modeling.[13,252–255] The advantage of this approach is that it requires only a single first-principles calculation for each surface configuration. However, the linear free energy approximation amounts to neglecting the change in charge of the surface + adsorbate as a function of electrode potential, setting it equal to the charge state of the single calculation performed.

The linearized free energy CHE approach is the first term in a Taylor expansion of the grand free energy with respect to either the electrode potential or the surface charge. As a function of surface charge, the linear coefficient of the grand free energy is the work function of the performed calculation. This expansion can be carried to higher orders to mitigate the constant-charge approximation discussed above.[17,256–260] The next lowest-order correction captures the linear change in potential with charge and corresponds to a constant (inverse) capacitance. This corresponds to a quadratic energy term accounting for the capacitive energy of changing the charge of the electrochemical double layer.

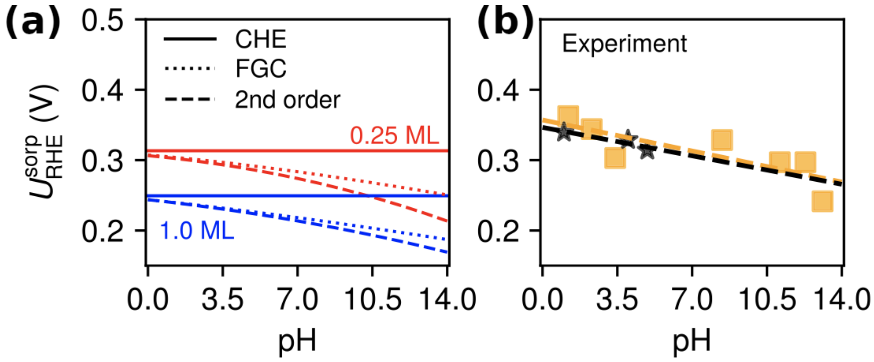

Figure 15: (a) Hydrogen binding on Pt(111), with hydrogen coverage of 1/4 monolayer(red) and 1 monolayer(blue). Full grand canonical (FGC) and second order models produce hydrogen binding curves as a function of pH that are similar to those measured from experiment (b), whereas the computational hydrogen electrode results do not vary with pH. (Adapted from Ref. 256. Copyright 2020 Springer Nature under (CC 4.0).)

Using this Taylor expansion, Ref. 256 analyzes proton adsorption at metal surfaces as a function of potential using the computational hydrogen electrode (first order), a constant inverse capacitance (second order), and the full grand canonical free energy, shown in Figure 15. The CHE approximation will predict a constant potential of H adsorption with respect to the reversible hydrogen electrode (RHE), independent of pH, essentially not distinguishing between adsorption and electrosorption. Second order and grand-canonical models predict adsorption variation with potential, which appear to qualitatively reproduce experimental trends for H on Pt(111).

While the perturbative approach can improve on the CHE approximation, the accuracy of using single DFT calculations to predict electrochemical properties can be limited by the electrolyte description (such as using a continuum solvation model) and the effects of surface charging. Explicitly including electrolyte species and searching the space of surface structures, as discussed in the previous section, may be necessary in many cases. For instance, unlike the good agreement for Pt(111) shown in Figure 15, Ref. 256 finds poor agreement with experimental trends for Pt(100) bridge site H-adsorption even for the explicit potential-dependent calculations. In fact, the variation of H adsorption on Pt step edges is caused not by charging the H, which would be captured by the potential-dependent DFT calculations, but rather by the displacement of coadsorbing cations, OH, and water from the step edge.[261] Such effects require the explicit inclusion of these co-adsorbed species in the electronic structure calculation, introducing the challenges of determining surface-bound and electrolyte structures discussed previously in Sections 5.1 and 5.2.

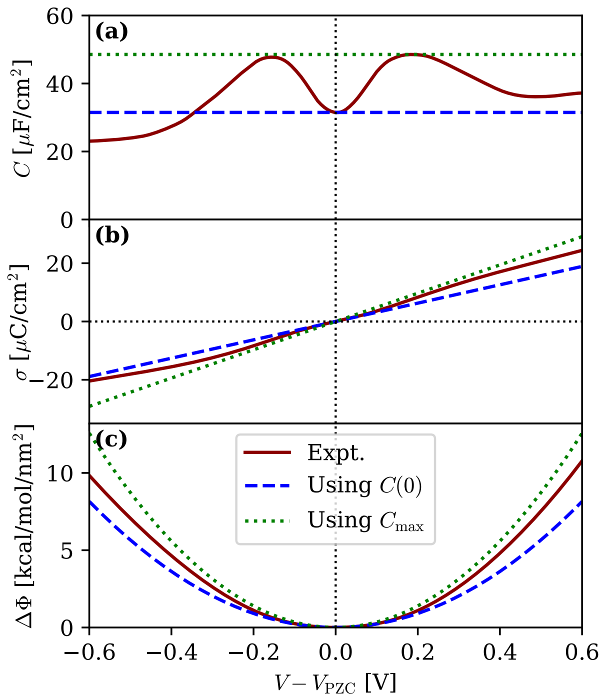

Figure 16: a) The experimental capacitance of Ag(100) in aqueous solution of 0.1 mol/L KPF_6 (solid red), from Ref. 262, with the capacitance maximum (green dots) and the value at the PZC (blue dashes) marked. b) Surface charge evaluated using the capacitance from experiment (solid red), the maximum (green dots) and the PZC (blue dashes). c) the change in surface free energy relative to the PZC using the three capacitances defined above.

Similarly, the effects of surface charging depend on several factors that are challenging to predict. First, perturbative approaches reduce in accuracy when moving away from the potential or charge of the reference calculation because they rely on the capacitance remaining constant over a wide potential range. To illustrate this, Figure 16 compares the variation of surface charge and energy of an Ag(100) surface with potential predicted from the experimental capacitance, using a constant equal to the PZC local-minimum value and using a constant equal to the maximum capacitance. As expected, the error in the surface energy caused by estimating the capacitance is small near the PZC and increases away from it, bounded by the minimum and the maximum capacitance approximations. Note that the energy errors can approach a kcal/mol/nm^2 over a potential difference of just 0.5 eV, which could be significant for predictions for reaction kinetics at the surface. A further complication is that the potential difference relative to the PZC, and hence, the severity of the above approximation, may be unknown. Specifically, the PZC is close to the work function for weak electrode-electrolyte interactions, but may be strongly offset from the work function for strong interactions and difficult to identify in both theory and experiment.[41]

The capacitance variations discussed so far are only because of the electrolyte contributions; changes in surface coverage can lead to even more drastic changes in capacitance. For example, the capacitance of Pt surface can experimentally change by a factor of two to three upon coverage by CO due to a change in hydrophobicity of the surface;[118] this is not captured by any of the standard electrochemical continuum solvation models automatically.[248,263] See Ref. 2 for further details on the variation of differential capacitance with potential and adsorbates.

Finally, changes in the surface geometry can also be important in certain potential ranges. As a concrete example, consider two metal electrodes with adsorbates that are similar under vacuum conditions: Pt(111) saturated with CO, and Cu(100) with c(2x2) Cl. These two surface configurations have work functions of 5.6 eV[264] and 5.7 eV respectively,[265,266] are both hydrophobic in aqueous electrolytes,[267] and have similar capacitance values of 11 μF/cm^2 at 0.4 V SHE[118,268] and 16 μF/cm^2 near 0 V vs SHE[228] respectively. However, under the same, near 0 V SHE electrochemical conditions, the two surfaces display very different behavior. The CO is nearly neutral, and does not significantly change bond length relative to vacuum, as demonstrated from Stark effect experiments. In contrast, the Cu-Cl bond increases 0.3 Å relative to vacuum conditions, and the Cl becomes highly charged. The key difference is that the Cu-Cl bond is very polar, so when the surface is charged, the bond lengthens, producing a larger surface dipole.[228] This example demonstrates that even when the work function, hydrophobicity, and capacitance of surfaces are very similar, their properties under electrochemical conditions can differ drastically. Such subtle effects underscore the need to carefully analyze the interplay of electronic structure and atomic geometry at the electrochemical interface.

6 Outlook

Computational electrochemistry using atomistic and electronic methods has rapidly progressed over the last few decades towards accurate and realistic simulations of complex charged interfaces. However, a compromise must still be made between the accuracy of simulations along the electron and atom-configuration axes of Figure 1. Future methodological advances should lessen the severity of this compromise by increasing accuracy achievable at fixed computational cost.

Along the electron axis, machine-learned force fields and empirical corrections allow low-cost energy evaluations for each configuration without sacrificing accuracy, which facilitates better structure searches and reaction energy predictions. Additionally, higher levels of *ab initio* theory such as RPA and QMC that increase the accuracy of electronic structure calculations are becoming less computationally expensive. These strategies can be combined together to achieve higher accuracy simulations for nearly equivalent computational cost. For example, RPA simulations of select systems can be used to develop machine-learned corrections to DFT predictions. Alternately, embedding methods can focus the computational expense of a higher-level method on a relevant subsystem, another promising direction for future electrochemical simulations.

Along the atomic axis, enhanced sampling methods reduce the number of energy evaluations required to capture long time-scale processes. Machine learning techniques can play a key role in further short-circuiting energy evaluations and MD time evolution to reach longer simulated times.[269,270] Recent machine-learned potentials that additionally predict charge distributions accounting for nonlocal charge transfers will be particularly important for electrochemical simulations including electrode potential effects. Coupled with increased computational power and the accuracy advances along the electron axis, this can lead to electrochemical simulations that approach realistic time and length scales.

Lastly, with the improved accuracy and efficiency of electronic structure and molecular dynamics methods, new opportunities exist to combine these tools with one another. Systematic integration of these tools will lead to further improved accuracy of atomistic simulations of the electrochemical interface.

Biographies

Ravishankar Sundararaman

Ravishankar Sundararaman is an Associate Professor of Materials Science and Engineering at Rensselaer Polytechnic Institute. He received a Ph.D. in Physics from Cornell University in 2013, and was a postdoctoral fellow in the Joint Center for Artificial Photosynthesis at Caltech till 2016. His research group develops combined quantum-classical simulations facilitating first-principles materials design for electrochemical, plasmonic and nano-electronic applications, and leads the development of the JDFTx open-source software for such calculations. He is the recipient of the AIME Robert Lansing Hardy Award in 2020.

Derek Vigil-Fowler

Derek Vigil-Fowler is a Staff Scientist at the National Renewable Energy Laboratory. He received his Ph.D. in Physics from the University of California, Berkeley in 2015. His research targets high-fidelity simulation methods for materials physics and chemistry, especially post-DFT, high accuracy methods such as the GW approximation for electronic structure and random phase approximation (RPA) total energies for reaction energetics.

Kathleen Schwarz

Kathleen Schwarz is a Staff Scientist at the National Institute of Standards and Technology (NIST). She received her Ph.D. in Chemistry from Cornell University in 2014, and then carried out postdoctoral work through the National Research Council Postdoctoral Program at NIST. Her research focuses on computational investigation of the electrochemical double layer at an atomistic level, targeting fundamental challenges in corrosion, electrocatalysis and electrodeposition.

Acknowledgements

RS and DVF acknowledge funding from the Department of Energy (BES) under award number DE-SC0022247. We thank Prof. Y Z for useful suggestions on enhanced sampling methods.

References

(1) Bazant, M. Z.; Thornton, K.; Ajdari, A. Diffuse-Charge Dynamics in Electrochemical Systems. *Phys. Rev. E* **2004**, *70*, 021506.

(2) Schwarz, K.; Sundararaman, R. The Electrochemical Interface in First-Principles Calculations. *Surf. Sci. Rep.* **2020**, *75*, 100492.

(3) Pham, T. A.; Lee, D.; Schwegler, E.; Galli, G. Interfacial Effects on the Band Edges of Functionalized Si Surfaces in Liquid Water. *J. Am. Chem. Soc.* **2014**, *136*, 17071–17077.

(4) Dorothea, G.; Marc, D.; Patrick, R. The GW Compendium: A Practical Guide to Theoretical Photoemission Spectroscopy. *Front. Chem.* **2019**, *7*, 377.

(5) Feibelman, P. J.; Hammer, B.; Norskov, J. K.; Wagner, F.; Scheffler, M.; Stumpf, R.; Watwe, R.; Dumesic, J. The CO/Pt(111) Puzzle. *J. Phys. Chem. B* **2001**, *105*, 4018–4025.

(6) Schimka, L.; Harl, J.; Stroppa, A.; Grüneis, A.; Marsman, M.; Mittendorfer, F.; Kresse, G. Accurate Surface and Adsorption Energies From Many-Body Perturbation Theory. *Nat. Mater.* **2010**, *9*, 741–744.

(7) Cheng, J.; Sprik, M. Alignment of Electronic Energy Levels at Electrochemical Interfaces. *Phys. Chem. Chem. Phys.* **2012**, *14*, 11245–11267.

(8) Baskin, A.; Prendergast, D. Improving Continuum Models to Define Practical Limits for Molecular Models of Electrified Interfaces. *J. Electrochem. Soc.* **2017**, *164*, E3438–E3447.

(9) Baskin, A.; Prendergast, D. Exploring Chemical Speciation at Electrified Interfaces Using Detailed Continuum Models. *J. Chem. Phys.* **2019**, *150*, 041725.

(10) Groß, A. *Surface and Interface Science*; John Wiley & Sons, Ltd, 2020; Chapter 56, pp 471–515.

(11) Tavernelli, I.; Vuilleumier, R.; Sprik, M. Ab Initio Molecular Dynamics for Molecules with Variable Numbers of Electrons. *Phys. Rev. Lett.* **2002**, *88*, 213002.

(12) Bonne, N.; Morishita, T.; Sugino, O.; Otani, M. First-Principles Molecular Dynamics at a Constant Electrode Potential. *Phys. Rev. Lett.* **2012**, *109*, 266101.

(13) Tripkovic, V.; Bjorketun, M. E.; Skulason, E.; Rossmeisl, J. Standard Hydrogen Electrode and Potential of Zero Charge in Density Functional Calculations. *Phys. Rev. B* **2011**, *84*, 115452.

(14) Cheng, J.; Sprik, M. Aligning Electronic Energy Levels at the TiO_2/H_2O Interface. *Phys. Rev. B* **2010**, *82*, 081406.

(15) Bouzid, A.; Pasquarello, A. Atomic-Scale Simulation of Electrochemical Processes at Electrode/Water Interfaces under Referenced Bias Potential. *J. Phys. Chem. Lett.* **2018**, *9*, 1880–1884.

(16) Le, J.-B.; Cheng, J. Modeling Electrochemical Interfaces From Ab Initio Molecular Dynamics: Water Adsorption on Metal Surfaces at Potential of Zero Charge. *Curr. Opin. Electrochem.* **2020**, *19*, 129–136.

(17) Ringe, S.; Hörmann, N. G.; Oberhofer, H.; Reuter, K. Implicit Solvation Methods for Catalysis at Electrified Interfaces. *Chem. Rev.* **2021**, *Articles ASAP*, DOI: 10.1021/acs.chemrev.1c00675.

(18) Dufils, T.; Jeanmairet, G.; Rotenberg, B.; Sprik, M.; Salanne, M. Simulating Electrochemical Systems by Combining the Finite Field Method with a Constant Potential Electrode. *Phys. Rev. Lett.* **2019**, *123*, 195501.

(19) Yang, X.-H.; Zhuang, Y.-B.; Zhu, J.-X.; Le, J.-B.; Cheng, J. Recent Progress on Multiscale Modeling of Electrochemistry. *Wiley Interdiscip. Rev. Comput. Mol. Sci* **2021**, e1559.

(20) Zhang, C.; Sayer, T.; Hutter, J.; Sprik, M. Modelling Electrochemical Systems With Finite Field Molecular Dynamics. *J. Phys. Energy* **2020**, *2*, 032005.

(21) Shandilya, A.; Schwarz, K.; Sundararaman, R. Interfacial Water Asymmetry at Ideal Electrochemical Interfaces. *J. Chem. Phys.* **2022**, *156*, 014705.

(22) Li, C.-Y.; Le, J.-B.; Wang, Y.-H.; Chen, S.; Yang, Z.-L.; Li, J.-F.; Cheng, J.; Tian, Z.-Q. In Situ Probing Electrified Interfacial Water Structures at Atomically Flat Surfaces. *Nat. Mater.* **2019**, *18*, 697–701.

(23) Vanzo, D.; Bratko, D.; Luzar, A. Nanoconfined Water Under Electric Field at Constant Chemical Potential Undergoes Electrostriction. *J. Chem. Phys.* **2014**, *140*, 074710.

(24) Kornyshev, A. A. Double-Layer in Ionic Liquids: Paradigm Change? *J. Phys. Chem. B* **2007**, *111*, 5545–5557.

(25) Georgi, N.; A.A.Kornyshev,; M.V.Fedorov, The Anatomy of the Double Layer and Capacitance in Ionic Liquids with Anisotropic Ions: Electrostriction vs. Lattice Saturation. *J. Electroanal. Chem.* **2010**, *649*, 261–267.

(26) Jiang, G.; Cheng, C.; Li, D.; Liu, J. Z. Molecular Dynamics Simulations of the Electric Double Layer Capacitance of Graphene Electrodes in Mono-Valent Aqueous Electrolytes. *Nano Res.* **2016**, *9*, 174–186.

(27) Hu, Z.; Vatamanu, J.; Borodin, O.; Bedrov, D. A Molecular Dynamics Simulation Study of the Electric Double Layer and Capacitance of [BMIM][PF6] and [BMIM][BF4] Room Temperature Ionic Liquids Near Charged Surfaces. *Phys. Chem. Chem. Phys.* **2013**, *15*, 14234–14247.

(28) Valentini, P.; Schwartzentruber, T. E.; Cozmuta, I. ReaxFF Grand Canonical Monte Carlo Simulation of Adsorption and Dissociation of Oxygen on Platinum (111). *Surf. Sci.* **2011**, *605*, 1941–1950.

(29) Jung, C. K.; Braunwarth, L.; Jacob, T. Grand Canonical ReaxFF Molecular Dynamics Simulations for Catalytic Reactions. *J. Chem. Theory Comput.* **2019**, *15*, 5810–5816.

(30) Hansen, M. H.; Rossmeisl, J. pH in Grand Canonical Statistics of an Electrochemical Interface. *J. Phys. Chem. C* **2016**, *120*, 29135–29143.

(31) Andrade, M. F. C.; Ko, H.-Y.; Car, R.; Selloni, A. Structure, Polarization, and Sum Frequency Generation Spectrum of Interfacial Water on Anatase TiO2. *J. Phys. Chem. Lett.* **2018**, *9*, 6716–6721.

(32) Zhang, Y.; Stirnemann, G.; Hynes, J. T.; Laage, D. Water Dynamics at Electrified

Graphene Interfaces: a Jump Model Perspective. *Phys. Chem. Chem. Phys.* **2020**, *22*, 10581–10591.

(33) Zhang, Y.; de Aguiar, H. B.; Hynes, J. T.; Laage, D. Water Structure, Dynamics, and Sum-Frequency Generation Spectra at Electrified Graphene Interfaces. *J. Phys. Chem. Lett.* **2020**, *11*, 624–631.

(34) Limmer, D. T.; Willard, A. P.; Madden, P. A.; Chandler, D. Water Exchange at a Hydrated Platinum Electrode is Rare and Collective. *J. Phys. Chem. C* **2015**, *119*, 24016–24024.

(35) Willard, A. P.; Limmer, D. T.; Madden, P. A.; Chandler, D. Characterizing Heterogeneous Dynamics at Hydrated Electrode Surfaces. *J. Chem. Phys.* **2013**, *138*, 184702.

(36) Limmer, D. T.; Willard, A. P.; Madden, P.; Chandler, D. Hydration of Metal Surfaces Can be Dynamically Heterogeneous and Hydrophobic. *Proc. Natl. Acad. Sci. U.S.A.* **2013**, *110*, 4200–4205.

(37) Berendsen, H. J. C.; Grigera, J. R.; Straatsma, T. P. The Missing Term in Effective Pair Potentials. *J. Phys. Chem.* **1987**, *91*, 6269.

(38) Fyta, M.; Netz, R. R. Ionic Force Field Optimization Based on Single-Ion and Ion-Pair Solvation Properties: Going Beyond Standard Mixing Rules. *J. Chem. Phys.* **2012**, *136*, 124103.

(39) Plimpton, S. Fast Parallel Algorithms for Short-Range Molecular Dynamics. *J. Comput. Phys.* **1995**, *117*, 1–19.

(40) Sakong, S.; Forster-Tonigold, K.; Groß, A. The Structure of Water at a Pt(111) Electrode and the Potential of Zero Charge Studied From First Principles. *J. Chem. Phys.* **2016**, *144*, 194701.

(41) Le, J.; Iannuzzi, M.; Cuesta, A.; Cheng, J. Determining Potentials of Zero Charge of Metal Electrodes versus the Standard Hydrogen Electrode from Density-Functional-Theory-Based Molecular Dynamics. *Phys. Rev. Lett.* **2017**, *119*, 016801.

(42) Yang, G.; Akhade, S. A.; Chen, X.; Liu, Y.; Lee, M.-S.; Glezakou, V.-A.; Rousseau, R.; Lercher, J. A. The Nature of Hydrogen Adsorption on Platinum in the Aqueous Phase. *Angew. Chem. Int. Ed.* **2019**, *58*, 3527–3532.

(43) Ciccotti, G.; Ferrario, M. Blue Moon Approach to Rare Events. *Molec. Simul.* **2004**, *30*, 787–793.

(44) Collinge, G.; Yuk, S. F.; Nguyen, M.-T.; Lee, M.-S.; Glezakou, V.-A.; Rousseau, R. Effect of Collective Dynamics and Anharmonicity on Entropy in Heterogenous Catalysis: Building the Case for Advanced Molecular Simulations. *ACS Catal.* **2020**, *10*, 9236–9260.

(45) Cheng, T.; Fortunelli, A.; III, W. A. G. Reaction Intermediates During Operando Electrocatalysis Identified From Full Solvent Quantum Mechanics Molecular Dynamics. *Proc. Natl. Acad. Sci. U.S.A.* **2019**, *116*, 7718–7722.

(46) Lin, S.-T.; Blanco, M.; III, W. A. G. The Two-Phase Model for Calculating Thermodynamic Properties of Liquids From Molecular Dynamics: Validation for the Phase Diagram of Lennard-Jones Fluids. *J. Chem. Phys.* **2003**, *119*, 11792.

(47) Andrade, M. F. C.; Ko, H.-Y.; Zhang, L.; Car, R.; Selloni, A. Free Energy of Proton Transfer at the Water–TiO_2 Interface from Ab Initio Deep Potential Molecular Dynamics. *Chem. Sci.* **2020**, *11*, 2335–2341.

(48) Laio, A.; Gervasio, F. L. Metadynamics: A Method to Simulate Rare Events and Reconstruct the Free Energy in Biophysics, Chemistry and Material Science. *Rep. Prog. Phys* **2008**, *71*, 126601.

(49) Barducci, A.; Bussi, G.; Parrinello, M. Well-Tempered Metadynamics: A Smoothly Converging and Tunable Free-Energy Method. *Phys. Rev. Lett.* **2008**, *100*, 020603.

(50) Barducci, A.; Bonomi, M.; Parrinello, M. Metadynamics. *Wiley Interdiscip. Rev. Comput. Mol. Sci.* **2011**, *1*, 826–843.

(51) Reocreux, R.; Girel, E.; Clabaut, P.; Tuel, A.; Besson, M.; Chaumonnot, A.; Cabiac, A.; Sautet, P.; Michel, C. Reactivity of Shape-Controlled Crystals and Metadynamics Simulations Locate the Weak Spots of Alumina in Water. *Nat. Commun.* **2019**, *10*, 3139.

(52) Piccini, G.; Lee, M.-S.; Yuk, S. F.; Zhang, D.; Collinge, G.; Kollias, L.; Nguyen, M.-T.; Glezakou, V.-A.; Rousseau, R. Ab Initio Molecular Dynamics With Enhanced Sampling in Heterogeneous Catalysis. *Catal. Sci. Technol.* **2022**,

(53) Yang, Y. I.; Shao, Q.; Zhang, J.; Yang, L.; Gao, Y. Q. Enhanced Sampling in Molecular Dynamics. *J. Chem. Phys.* **2019**, *151*, 070902.

(54) Hamelberg, D.; de Oliveira, C. A. F.; McCammon, J. A. Sampling of Slow Diffusive Conformational Transitions With Accelerated Molecular Dynamics. *J. Chem. Phys.* **2007**, *127*, 155102.

(55) Voter, A. F.; Montalenti, F.; Germann, T. C. Extending the Time Scale in Atomistic Simulation of Materials. *Annu. Rev. Mater. Res* **2002**, *32*, 321–346.

(56) Hamelberg, D.; Mongan, J.; McCammon, J. A. Accelerated Molecular Dynamics: A Promising and Efficient Simulation Method for Biomolecules. *J. Chem. Phys.* **2004**, *120*, 11919.

(57) Bernardi, R. C.; Melo, M. C.; Schulten, K. Enhanced Sampling Techniques in Molecular Dynamics Simulations of Biological Systems. *Biochim. Biophys. Acta Gen. Subj.* **2015**, *1850*, 872–877.

(58) Comer, J.; Gumbart, J. C.; Hénin, J.; Lelièvre, T.; Pohorille, A.; Chipot, C. The Adaptive Biasing Force Method: Everything You Always Wanted To Know but Were Afraid To Ask. *J. Phys. Chem. B* **2015**, *119*, 1129–1151.

(59) Riniker, S. Fixed-Charge Atomistic Force Fields for Molecular Dynamics Simulations in the Condensed Phase: An Overview. *J. Chem. Inf. Model.* **2018**, *58*, 565–578.

(60) Dommert, F.; Wendler, K.; Berger, R.; Site, L. D.; Holm, C. Force Fields for Studying the Structure and Dynamics of Ionic Liquids: A Critical Review of Recent Developments. *ChemPhysChem* **2012**, *13*, 1625–1637.

(61) Huang, L.; Roux, B. Automated Force Field Parameterization for Nonpolarizable and Polarizable Atomic Models Based on Ab Initio Target Data. *J. Chem. Theory Comput.* **2013**, *9*, 3543–3556.

(62) Smith, W. R.; Nezbeda, I.; Kolafa, J.; Moučka, F. Recent Progress in the Molecular Simulation of Thermodynamic Properties of Aqueous Electrolyte Solutions. *Fluid Phase Equilib.* **2018**, *466*, 19–30.

(63) Saric, D.; Kohns, M.; Vrabec, J. Dielectric Constant and Density of Aqueous Alkali Halide Solutions by Molecular Dynamics: A Force Field Assessment. *J. Chem. Phys.* **2020**, *152*, 164502.

(64) Geada, I. L.; Ramezani-Dakhel, H.; Jamil, T.; Sulpizi, M.; Heinz, H. Insight Into Induced Charges at Metal Surfaces and Biointerfaces Using a Polarizable Lennard–Jones Potential. *Nat. Commun.* **2018**, *9*, 716.

(65) Halgren, T. A.; Damm, W. Polarizable Force Fields. *Current Opin. Struct. Bio.* **2001**, *11*, 236 – 242.

(66) Bedrov, D.; Piquemal, J.-P.; Borodin, O.; Jr., A. D. M.; Roux, B.; Schröder, C.

Molecular Dynamics Simulations of Ionic Liquids and Electrolytes Using Polarizable Force Fields. *Chem. Rev.* **2019**, *119*, 7940–7995.

(67) Rappe, A. K.; Goddard, W. A. Charge Equilibration for Molecular Dynamics Simulations. *J. Phys. Chem.* **1991**, *95*, 3358–3363.

(68) Senftle, T. P.; Hong, S.; Islam, M. M.; Kylasa, S. B.; Zheng, Y.; Shin, Y. K.; Junkermeier, C.; Engel-Herbert, R.; Janik, M. J.; Aktulga, H. M. et al. The ReaxFF Reactive Force-Field: Development, Applications and Future Directions. *npj Comput. Mater.* **2016**, *2*, 15011.

(69) Liang, T.; Shan, T.-R.; Cheng, Y.-T.; Devine, B. D.; Noordhoek, M.; Li, Y.; Lu, Z.; Phillpot, S. R.; Sinnott, S. B. Classical Atomistic Simulations of Surfaces and Heterogeneous Interfaces With the Charge-Optimized Many Body (COMB) Potentials. *Mater. Sci. Eng.: R: Rep.* **2013**, *74*, 255–279.

(70) Ko, T. W.; Finkler, J. A.; Goedecker, S.; Behler, J. A Fourth-Generation High-Dimensional Neural Network Potential with Accurate Electrostatics Including Non-Local Charge Transfer. *Nat. Commun.* **2021**, *12*, 398.

(71) Jinnouchi, R.; Karsai, F.; Verdi, C.; Asahi, R.; Kresse, G. Descriptors Representing Two- and Three-Body Atomic Distributions and Their Effects on the Accuracy of Machine-Learned Inter-Atomic Potentials. *J. Chem. Phys.* **2020**, *152*, 234102.

(72) Unke, O. T.; Chmiela, S.; Sauceda, H. E.; Gastegger, M.; Poltavsky, I.; Schütt, K. T.; Tkatchenko, A.; Müller, K.-R. Machine Learning Force Fields. *Chemical Reviews* **2021**, *121*, 10142–10186.

(73) Behler, J. Four Generations of High-Dimensional Neural Network Potentials. *Chem. Rev.* **2021**, *121*, 10037–10072.

(74) Staacke, C. G.; Heenen, H. H.; Scheurer, C.; Csányi, G.; Reuter, K.; Margraf, J. T. On the Role of Long-Range Electrostatics in Machine-Learned Interatomic Potentials for Complex Battery Materials. *ACS Appl. Energy Mater.* **2021**, *4*, 12562–12569.

(75) Eckhoff, M.; Behler, J. Insights into Lithium Manganese Oxide–Water Interfaces Using Machine Learning Potentials. *J. Chem. Phys.* **2021**, *155*, 244703.

(76) Xie, X.; Persson, K. A.; Small, D. W. Incorporating Electronic Information into Machine Learning Potential Energy Surfaces via Approaching the Ground-State Electronic Energy as a Function of Atom-Based Electronic Populations. *J. Chem. Theory Comput.* **2020**, *16*, 4256–4270.

(77) Metcalf, D. P.; Jiang, A.; Spronk, S. A.; Cheney, D. L.; Sherrill, C. D. Electron-Passing Neural Networks for Atomic Charge Prediction in Systems with Arbitrary Molecular Charge. *J. Chem. Inf. Model.* **2021**, *61*, 115–122.

(78) Ko, T. W.; Finkler, J. A.; Goedecker, S.; Behler, J. General-Purpose Machine Learning Potentials Capturing Nonlocal Charge Transfer. *Acc. Chem. Res.* **2021**, *54*, 808–817.

(79) Ghasemi, S. A.; Hofstetter, A.; Saha, S.; Goedecker, S. Interatomic Potentials for Ionic Systems with Density Functional Accuracy Based on Charge Densities Obtained by a Neural Network. *Phys. Rev. B* **2015**, *92*, 045131.

(80) Grisafi, A.; Ceriotti, M. Incorporating Long-Range Physics in Atomic-Scale Machine Learning. *J. Chem. Phys.* **2019**, *151*, 204105.

(81) Jinnouchi, R.; Miwa, K.; Karsai, F.; Kresse, G.; Asahi, R. On-the-Fly Active Learning of Interatomic Potentials for Large-Scale Atomistic Simulations. *J. Phys. Chem. Lett.* **2020**, *11*, 6946–6955.

(82) Vandermause, J.; Torrisi, S. B.; Batzner, S.; Xie, Y.; Sun, L.; Kolpak, A. M.; Kozin-

sky, B. On-the-Fly Active Learning of Interpretable Bayesian Force Fields for Atomistic Rare Events. *npj Comput. Mater.* **2020**, *6*, 20.

(83) Schran, C.; Thiemann, F. L.; Rowe, P.; Mülle, E. A.; Marsalek, O.; Michaelides, A. Machine Learning Potentials for Complex Aqueous Systems Made Simple. *Proc. Natl. Acad. Sci. U.S.A.* **2021**, *118*, e2110077118.

(84) Sundararaman, R.; Goddard III, W. A.; Arias, T. A. Grand Canonical Electronic Density-Functional Theory: Algorithms and Applications to Electrochemistry. *J. Chem. Phys.* **2017**, *146*, 114104.

(85) Wang, Z.; Yang, Y.; Olmsted, D. L.; Asta, M.; Laird, B. B. Evaluation of the Constant Potential Method in Simulating Electric Double-Layer Capacitors. *J. Chem. Phys.* **2014**, *141*, 184102.

(86) Merlet, C.; Péan, C.; Rotenberg, B.; Madden, P. A.; Simon, P.; Salanne, M. Simulating Supercapacitors: Can We Model Electrodes As Constant Charge Surfaces? *J. Phys. Chem. Lett.* **2013**, *4*, 264–268.

(87) Siepmann, J. I.; Sprik, M. Influence of Surface Topology and Electrostatic Potential on Water/Electrode Systems. *J. Chem. Phys.* **1995**, *102*, 511.

(88) Reed, S. K.; Lanning, O. J.; Madden, P. A. Electrochemical Interface Between an Ionic Liquid and a Model Metallic Electrode. *J. Chem. Phys.* **2007**, *126*, 084704.

(89) Vatamanu, J.; Bedrov, D.; Borodin, O. On the Application of Constant Electrode Potential Simulation Techniques in Atomistic Modelling of Electric Double Layers. *Mol. Simul.* **2017**, *43*, 838–849.

(90) Coretti, A.; Scalfi, L.; Bacon, C.; Rotenberg, B.; Vuilleumier, R.; Ciccotti, G.; Salanne, M.; Bonella, S. Mass-Zero Constrained Molecular Dynamics for Electrode Charges in Simulations of Electrochemical Systems. *J. Chem. Phys.* **2020**, *152*, 194701.

(91) Cornell, W. D.; Cieplak, P.; Bayly, C. I.; Gould, I. R.; Merz, K. M.; Ferguson, D. M.; Spellmeyer, D. C.; Fox, T.; Caldwell, J. W.; Kollman, P. A. A Second Generation Force Field for the Simulation of Proteins, Nucleic Acids, and Organic Molecules. *J. Am. Chem. Soc.* **1995**, *117*, 5179–5197.

(92) MacKerell, A. D.; Bashford, D.; Bellott, M.; Dunbrack, R. L.; Evanseck, J. D.; Field, M. J.; Fischer, S.; Gao, J.; Guo, H.; Ha, S. et al. All-Atom Empirical Potential for Molecular Modeling and Dynamics Studies of Proteins. *J. Phys. Chem. B* **1998**, *102*, 3586–3616.

(93) Abascal, J. L. F.; Vega, C. A General Purpose Model for the Condensed Phases of Water: TIP4P/2005. *J. Chem. Phys.* **2005**, *123*, 234505.

(94) Wernersson, E.; Kjellander, R. On the Effect of Image Charges and Ion-Wall Dispersion Forces on Electric Double Layer Interactions. *J. Chem. Phys.* **2006**, *125*, 154702.

(95) Iori, F.; Corni, S. Including Image Charge Effects in the Molecular Dynamics Simulations of Molecules on Metal Surfaces. *J. Comput. Chem.* **2008**, *29*, 1656–1666.

(96) Steinmann, S. N.; Fleurat-Lessard, P.; Gotz, A. W.; Michel, C.; de Morais, R. F.; Sautet, P. Molecular Mechanics Models for the Image Charge, A Comment on "Including Image Charge Effects in the Molecular Dynamics Simulations of Molecules on Metal Surfaces". *J. Comput. Chem.* **2017**, *38*, 2127–2129.

(97) Gingrich, T. R.; Wilson, M. On the Ewald Summation of Gaussian Charges for the Simulation of Metallic Surfaces. *Chem. Phys. Lett.* **2010**, *500*, 178–183.

(98) Marin-Laflèche, A.; Haefele, M.; Scalfi, L.; Coretti, A.; Dufils, T.; Jeanmairet, G.; Reed, S. K.; Serva, A.; Berthin, R.; Bacon, C. et al. MetalWalls: A Classical Molecular Dynamics Software Dedicated to the Simulation of Electrochemical Systems. *J. Open Source Softw.* **2020**, *5*, 2373.

(99) Burt, R.; Birkett, G.; Zhao, X. S. A Review of Molecular Modelling of Electric Double Layer Capacitors. *Phys. Chem. Chem. Phys.* **2014**, *16*, 6519–6538.

(100) Haskins, J. B.; Lawson, J. W. Evaluation of Molecular Dynamics Simulation Methods for Ionic Liquid Electric Double Layers. *J. Chem. Phys.* **2016**, *144*, 184707.

(101) Aragones, J. L.; Sanz, E.; Valeriani, C.; Vega, C. Calculation of the Melting Point of Alkali Halides by Means of Computer Simulations. *J. Chem. Phys.* **2012**, *137*, 104507.

(102) Vatamanu, J.; Borodin, O.; Smith, G. D. Molecular Simulations of the Electric Double Layer Structure, Differential Capacitance, and Charging Kinetics for N-Methyl-N-propylpyrrolidinium Bis(fluorosulfonyl)imide at Graphite Electrodes. *J. Phys. Chem. B* **2011**, *115*, 3073–3084.

(103) Limmer, D. T.; Merlet, C.; Salanne, M.; Chandler, D.; Madden, P. A.; van Roij, R.; Rotenberg, B. Charge Fluctuations in Nanoscale Capacitors. *Phys. Rev. Lett.* **2013**, *111*, 106102.

(104) Scalfi, L.; Limmer, D. T.; Coretti, A.; Bonella, S.; Madden, P. A.; Salanne, M.; Rotenberg, B. Charge Fluctuations From Molecular Simulations in the Constant-Potential Ensemble. *Phys. Chem. Chem. Phys.* **2020**, *22*, 10480–10489.

(105) Uralcan, B.; Aksay, I. A.; Debenedetti, P. G.; Limmer, D. T. Concentration Fluctuations and Capacitive Response in Dense Ionic Solutions. *J. Phys. Chem. Lett.* **2016**, *7*, 2333–2338.

(106) Demir, B.; Searles, D. J. Investigation of the Ionic Liquid Graphene Electric Double Layer in Supercapacitors Using Constant Potential Simulations. *Nanomaterials* **2020**, *10*, 2181.

(107) Petersen, M. K.; Kumar, R.; White, H. S.; Voth, G. A. A Computationally Efficient

Treatment of Polarizable Electrochemical Cells Held at a Constant Potential. *J. Phys. Chem. C* **2012**, *116*, 4903–4912.

(108) Dwelle, K. A.; Willard, A. P. Constant Potential, Electrochemically Active Boundary Conditions for Electrochemical Simulation. *J. Phys. Chem. C* **2019**, *123*, 24095–24103.

(109) Sundararaman, R.; Gunceler, D.; Arias, T. A. Weighted-Density Functionals for Cavity Formation and Dispersion Energies in Continuum Solvation Models. *J. Chem. Phys.* **2014**, *141*, 134105.

(110) Willard, A. P.; Reed, S. K.; Madden, P. A.; Chandler, D. Water at an Electrochemical Interface—A Simulation Study. *Faraday Discuss.* **2009**, *141*, 423–441.

(111) Kornyshev, A. A.; Luque, N. B.; Schmickler, W. Differential Capacitance of Ionic Liquid Interface With Graphite: The Story of Two Double Layers. *J. Solid State Electrochem.* **2014**, *18*, 1345–1349.

(112) Ruzanov, A.; Lembinen, M.; Jakovits, P.; Srirama, S. N.; Voroshylova, I. V.; Cordeiro, M. N. D. S.; Pereira, C. M.; Rossmeisl, J.; Ivaništšev, V. B. On the Thickness of the Double Layer in Ionic Liquids. *Phys. Chem. Chem. Phys.* **2018**, *20*, 10275–10285.

(113) Paek, E.; Pak, A. J.; Hwang, G. S. A Computational Study of the Interfacial Structure and Capacitance of Graphene in [BMIM][PF6] Ionic Liquid. *J. Electrochem. Soc.* **2013**, *160*, A1–A10.

(114) Ers, H.; Lembinen, M.; Mišin, M.; Seitsonen, A. P.; Fedorov, M. V.; Ivaništšev, V. B. Graphene–Ionic Liquid Interfacial Potential Drop from Density Functional Theory-Based Molecular Dynamics Simulations. *J. Phys. Chem. C* **2020**, *124*, 19548–19555.

(115) Shandilya, A.; Schwarz, K.; Sundararaman, R. Erratum: "Interfacial Water Asymmetry at Ideal Electrochemical Interfaces". *J. Chem. Phys.* **2022**, *156*, 129901.

(116) Shin, S.; Kim, D.; Bae, G.; Ringe, S.; Choi, H.; Lim, H.-K.; Choi, C. H.; Kim, H. On the Importance of the Electric Double Layer Structure in Aqueous Electrocatalysis. *Nat. Commun.* **2022**, *13*, 174.

(117) Scalfi, L.; Dufils, T.; Reeves, K. G.; Rotenberg, B.; Salanne, M. A Semiclassical Thomas–Fermi Model to Tune the Metallicity of Electrodes in Molecular Simulations. *J. Chem. Phys.* **2020**, *153*, 174704.

(118) Sundararaman, R.; Figueiredo, M. C.; Koper, M. T. M.; Schwarz, K. A. Electrochemical Capacitance of CO-Terminated Pt(111) Dominated by the CO–Solvent Gap. *J. Phys. Chem. Lett.* **2017**, *8*, 5344–5348.

(119) Chung, H. T.; Cullen, D. A.; Higgins, D.; Sneed, B. T.; Holby, E. F.; More, K. L.; Zelenay, P. Direct Atomic-Level Insight Into the Active Sites of a High-Performance PGM-Free ORR Catalyst. *Science* **2017**, *357*, 479–484.

(120) Singh, M. R.; Goodpaster, J. D.; Weber, A. Z.; Head-Gordon, M.; Bell, A. T. Mechanistic Insights Into Electrochemical Reduction of CO_2 over Ag Using Density Functional Theory and Transport Models. *Proc. Natl. Acad. Sci. U.S.A.* **2017**, *114*, E8812–E8821.

(121) Ha, M.-A.; Larsen, R. E. Multiple Reaction Pathways for the Oxygen Evolution Reaction May Contribute to IrO2 (110)'s High Activity. *J. Electrochem. Soc.* **2021**, *168*, 024506.

(122) Knirsch, K. C.; Berner, N. C.; Nerl, H. C.; Cucinotta, C. S.; Gholamvand, Z.; McEvoy, N.; Wang, Z.; Abramovic, I.; Vecera, P.; Halik, M. et al. Basal-Plane Functionalization of Chemically Exfoliated Molybdenum Disulfide by Diazonium Salts. *ACS Nano* **2015**, *9*, 6018–6030.

(123) Tang, Q.; Jiang, D. Mechanism of Hydrogen Evolution Reaction on 1T-MoS_2 from First Principles. *ACS Catal.* **2016**, *6*, 4953–4961.

(124) Parr, R.; Yang, W. *Density-Functional Theory of Atoms and Molecules*; Oxford University Press: New York, New York, 1989.

(125) Wellendorff, J.; Silbaugh, T. L.; Garcia-Pintos, D.; Nørskov, J. K.; Bligaard, T.; Studt, F.; T.Campbell, C. A Benchmark Database for Adsorption Bond Energies to Transition Metal Surfaces and Comparison to Selected DFT Functionals. *Surf. Sci.* **2015**, *640*, 36–44.

(126) Hensley, A. J. R.; Ghale, K.; Rieg, C.; Dang, T.; Anderst, E.; Studt, F.; Campbell, C. T.; McEwen, J.-S.; Xu, Y. DFT-Based Method for More Accurate Adsorption Energies: An Adaptive Sum of Energies from RPBE and vdW Density Functionals. *Phys. Chem. C* **2017**, *121*, 4937–4945.

(127) Gautier, S.; Steinmann, S. N.; Michel, C.; Fleurat-Lessard, P.; Sautet, P. Molecular Adsorption at Pt(111). How Accurate are DFT Functionals? *Phys. Chem. Chem. Phys.* **2015**, *17*, 28921–28930.

(128) Mahlberg, D.; Sakong, S.; Forster-Tonigold, K.; Groß, A. Improved DFT Adsorption Energies with Semiempirical Dispersion Corrections. *J. Chem. Theory Comput.* **2019**, *15*, 3250–3259.

(129) Blumenthal, L.; Kahk, J. M.; Sundararaman, R.; Tangney, P.; Lischner, J. Energy Level Alignment at Semiconductor–Water Interfaces from Atomistic and Continuum Solvation Models. **2017**, *7*, 43660.

(130) Huang, L.-F.; Rondinelli, J. M. Electrochemical Phase Diagrams of Ni From Ab Initio Simulations: Role of Exchange Interactions on Accuracy. *J. Phys.: Condens. Matter* **2017**, *29*, 475501.

(131) McDowell, S. A.; Amos, R. D.; Handy, N. C. Molecular Polarisabilities - A Comparison of Density Functional Theory With Standard Ab Initio Methods. *Chem. Phys. Lett.* **1995**, *235*, 1–4.

(132) Zhang, C.; Hutter, J.; Sprik, M. Computing the Kirkwood g-Factor by Combining Constant Maxwell Electric Field and Electric Displacement Simulations: Application to the Dielectric Constant of Liquid Water. *J. Phys. Chem. Lett.* **2016**, *7*, 2696–2701.

(133) Bonnet, N.; Marzari, N. Static Dielectric Permittivity of Ice from First Principles. *Phys. Rev. Lett.* **2014**, *113*, 245501.

(134) Schönherr, M.; Slater, B.; Hutter, J.; VandeVondele, J. Dielectric Properties of Water Ice, the Ice Ih/XI Phase Transition, and an Assessment of Density Functional Theory. *J. Phys. Chem. B* **2014**, *118*, 590–596.

(135) Gillan, M. J.; Alfè, D.; Michaelides, A. Perspective: How Good is DFT for Water? *J. Chem. Phys.* **2016**, *144*, 130901.

(136) Wagle, K.; Santra, B.; Bhattarai, P.; Shahi, C.; Pederson, M. R.; Jackson, K. A.; Perdew, J. P. Self-Interaction Correction in Water–Ion Clusters. *J. Chem. Phys.* **2021**, *154*, 094302.

(137) Lage-Estebanez, I.; Ruzanov, A.; de la Vega, J. M. G.; Fedorov, M. V.; Ivaništšev, V. B. Self-Interaction Error in DFT-Based Modelling of Ionic Liquids. *Phys. Chem. Chem. Phys.* **2016**, *18*, 2175–2182.

(138) Liu, J.; Liu, H.; Chen, H.; Du, X.; Zhang, B.; Hong, Z.; Sun, S.; Wang, W. Progress and Challenges Toward the Rational Design of Oxygen Electrocatalysts Based on a Descriptor Approach. *Adv Sci (Weinh)* **2020**, *7*, 1901614.

(139) Hammer, B.; Norskov, J. Why Gold is the Noblest of all the Metals. *Nature* **1995**, *376*, 238–240.

(140) Gao, W.; Chen, Y.; Li, B.; Liu, S.-P.; Liu, X.; Jiang, Q. Determining the Adsorption Energies of Small Molecules With the Intrinsic Properties of Adsorbates and Substrates. *Nat Commun* **2020**, *11*, 1196.

(141) Granda-Marulanda, L. P.; Rendoń-Calle, A.; Builes, S.; Illas, F.; Koper, M. T. M.; Calle-Vallejo, F. A Semiempirical Method to Detect and Correct DFT-Based Gas-Phase Errors and Its Application in Electrocatalysis. *ACS Catal.* **2020**, *10*, 6900–6907.

(142) Huzayyin, A.; Chang, J. H.; Lian, K.; Dawson, F. Interaction of Water Molecule with Au(111) and Au(110) Surfaces under the Influence of an External Electric Field. *J. Phys. Chem. C* **2014**, *118*, 3459–3470.

(143) Diaz, C.; Pijper, E.; Olsen, R. A.; Busnengo, H. F.; Auerbach, D. J.; Kroes, G. J. Chemically Accurate Simulation of a Prototypical Surface Reaction: H2 Dissociation on Cu(111). *Science* **2009**, *326*, 832–834.

(144) Ghassemi, E. N.; Somers, M. F.; Kroes, G.-J. Assessment of Two Problems of Specific Reaction Parameter Density Functional Theory: Sticking and Diffraction of H2 on Pt(111). *J. Phys. Chem. C* **2019**, *123*, 10406–10418.

(145) Tchakoua, T.; Smeets, E. W. F.; Somers, M.; Kroes, G.-J. Toward a Specific Reaction Parameter Density Functional for H2 + Ni(111): Comparison of Theory with Molecular Beam Sticking Experiments. *J. Phys. Chem. C* **2019**, *123*, 20420–20433.

(146) Smeets, E. W. F.; Kroes, G.-J. Designing New SRP Density Functionals Including Non-Local vdW-DF2 Correlation for H2 + Cu(111) and Their Transferability to H2 + Ag(111), Au(111) and Pt(111). *Phys. Chem. Chem. Phys.* **2021**, *23*, 7875–7901.

(147) Kroes, G.-J. Computational Approaches to Dissociative Chemisorption on Metals: Towards Chemical Accuracy. *Phys. Chem. Chem. Phys.* **2021**, *23*, 8962–9048.

(148) Mason, S. E.; Grinberg, I.; Rappe, A. M. First-Principles Extrapolation Method for Accurate CO Adsorption Energies on Metal Surfaces. *Phys. Rev. B* **2004**, *69*, 161401.

(149) Faber, F. A.; Hutchison, L.; Huang, B.; Gilmer, J.; Schoenholz, S. S.; Dahl, G. E.; Vinyals, O.; Kearnes, S.; Riley, P. F.; von Lilienfeld, O. A. Prediction Errors of Molecular Machine Learning Models Lower than Hybrid DFT Error. *J. Chem. Theory Comput.* **2017**, *13*, 5255–5264.

(150) Ramakrishnan, R.; Dral, P. O.; Rupp, M.; von Lilienfeld, O. A. Big Data Meets Quantum Chemistry Approximations: The Δ-Machine Learning Approach. *Journal of Chemical Theory and Computation* **2015**, *11*, 2087–2096.

(151) Bogojeski, M.; Vogt-Maranto, L.; Tuckerman, M.; Müller, K.-R.; Burke, K. Quantum Chemical Accuracy From Density Functional Approximations via Machine Learning. *Nat Commun* **2020**, *11*, 5223.

(152) Liu, P.; Verdi, C.; Karsai, F.; Kresse, G. Phase Transitions of Zirconia: Machine-Learned Force Fields Beyond Density Functional Theory. *https://arxiv.org/pdf/2109.06282.pdf* **2021**,

(153) Chehaibou, B.; Badawi, M.; Bučko, T.; Bazhirov, T.; Rocca, D. Computing RPA Adsorption Enthalpies by Machine Learning Thermodynamic Perturbation Theory. *J. Chem. Theory Comput.* **2019**, *15*, 6333–6342.

(154) Grimme, S. Semiempirical GGA-Type Density Functional Constructed With a Long-Range Dispersion Correction. *J. Comput. Chem.* **2006**, *27*, 1787–1799.

(155) Grimme, S.; Antony, J.; Ehrlich, S.; Krieg, H. A Consistent and Accurate Ab Initio Parametrization of Density Functional Dispersion Correction (DFT-D) for the 94 Elements H-Pu. *J. Chem. Phys.* **2010**, *132*, 154104.

(156) Tkatchenko, A.; Scheffler, M. Accurate Molecular Van der Waals Interactions From Ground-State Electron Density and Free-Atom Reference Data. *Phys. Rev. Lett.* **2009**, *102*, 73005.

(157) Dion, M.; Rydberg, H.; Schröder, E.; Langreth, D. C.; Lundqvist, B. I. Van der Waals Density Functional for General Geometries. *Phys. Rev. Lett.* **2004**, *92*, 246401.

(158) Wellendorff, J.; Lundgaard, K. T.; Møgelhøj, A.; Petzold, V.; Landis, D. D.; Nørskov, J. K.; Bligaard, T.; Jacobsen, K. W. Density Functionals for Surface Science: Exchange-Correlation Model Development With Bayesian Error Estimation. *Phys. Rev. B* **2012**, *85*, 235149.

(159) Berland, K.; Cooper, V. R.; Lee, K.; Schröder, E.; Thonhauser, T.; Hyldgaard, P.; Lundqvist, B. I. Van der Waals Forces in Density Functional Theory: A Review of the vdW-DF Method. *Rep. Prog. Phys* **2015**, *78*, 066501.

(160) Olsen, T.; Thygesen, K. S. Random Phase Approximation Applied to Solids, Molecules, and Graphene-Metal Interfaces: From Van der Waals to Covalent Bonding. *Phys. Rev. B* **2013**, *87*, 075111.

(161) Gaiduk, A. P.; Gustafson, J.; Gygi, F.; Galli, G. First-Principles Simulations of Liquid Water Using a Dielectric-Dependent Hybrid Functional. *J. Phys. Chem. Lett.* **2018**, *9*, 3068–3073.

(162) Zhang, C.; Wu, J.; Galli, G.; Gygi, F. Structural and Vibrational Properties of Liquid Water From Van der Waals Density Functionals. *J. Chem. Theory Comput.* **2011**, *7*, 3054–3061.

(163) Morawietz, T.; Singraber, A.; Dellago, C.; Behler, J. How Van der Waals Interactions Determine the Unique Properties of Water. *Proc. Natl. Acad. Sci. U.S.A.* **2016**, *113*, 8368–8373.

(164) Gerrits, N.; Smeets, E. W. F.; Vuckovic, S.; Powell, A. D.; Doblhoff-Dier, K.; Kroes, G.-J. Density Functional Theory for Molecule–Metal Surface Reactions: When Does the Generalized Gradient Approximation Get It Right, and What to Do If It Does Not. *J. Phys. Chem. Lett.* **2020**, *11*, 10552–10560.

(165) Perdew, J. P.; Zunger, A. Self-Interaction Correction to Density-Functional Approximations for Many-Electron Systems. *Phys. Rev. B* **1981**, *23*, 5048.

(166) Sharkas, K.; Wagle, K.; Santra, B.; Akter, S.; Zope, R. R.; Baruah, T.; Jackson, K. A.; Perdew, J. P.; Peralta, J. E. Self-Interaction Error Overbinds Water Clusters but Cancels in Structural Energy Differences. *Proc. Natl. Acad. Sci. U.S.A.* **2020**, *117*, 11283–11288.

(167) Dudarev, S. L.; Botton, G. A.; Savrasov, S. Y.; Humphreys, C. J.; Sutton, A. P. Electron-Energy-Loss Spectra and the Structural Stability of Nickel Oxide: An LSDA+U Study. *Phys. Rev. B* **1998**, *57*, 1505–1509.

(168) Himmetoglu, B.; Floris, A.; de Gironcoli, S.; Cococcioni, M. Hubbard-Corrected DFT Energy Functionals: The LDA+U Description of Correlated Systems. *Int. J. Quantum Chem.* **2013**, *114*, 14–49.

(169) Tolba, S. A.; Gameel, K. M.; Ali, B. A.; Almossalami, H. A.; Allam, N. K. In *Density Functional Calculations*; Yang, G., Ed.; IntechOpen: Rijeka, 2018; Chapter 1.

(170) Zhao, Q.; Kulik, H. J. Stable Surfaces That Bind Too Tightly: Can Range-Separated Hybrids or DFT+U Improve Paradoxical Descriptions of Surface Chemistry? *J. Phys. Chem. Lett.* **2019**, *10*, 5090–5098.

(171) Capdevila-Cortada, M.; Łodziana, Z.; López, N. Performance of DFT+U Approaches in the Study of Catalytic Materials. *ACS Catal.* **2016**, *6*, 8370–8379.

(172) Janesko, B. G. Replacing Hybrid Density Functional Theory: Motivation and Recent Advances. *Chem. Soc. Rev.* **2021**, *50*, 8470–8495.

(173) Becke, A. D. Density-Functional Thermochemistry. III. The Role of Exact Exchange. *J. Chem. Phys.* **1993**, *98*, 5648.

(174) Stephens, P. J.; Devlin, F. J.; Chabalowski, C. F.; Frisch, M. J. Ab Initio Calculation of Vibrational Absorption and Circular Dichroism Spectra Using Density Functional Force Fields. *J. Phys. Chem.* **1994**, *98*, 11623–11627.

(175) Heyd, J.; Scuseria, G. E. Hybrid Functionals Based on a Screened Coulomb Potential. *J. Chem. Phys.* **2003**, *118*, 8207–8215.

(176) Gerosa, M.; Bottani, C. E.; Caramella, L.; Onida, G.; Valentin, C. D.; Pacchioni, G. Electronic Structure and Phase Stability of Oxide Semiconductors: Performance of Dielectric-Dependent Hybrid Functional DFT, Benchmarked Against GW Band Structure Calculations and Experiments. *Phys. Rev. B* **2015**, *91*.

(177) Chen, W.; Miceli, G.; Rignanese, G.-M.; Pasquarello, A. Nonempirical Dielectric-Dependent Hybrid Functional With Range Separation for Semiconductors and Insulators. *Phys. Rev. Mater.* **2018**, *2*, 073803.

(178) Paier, J.; Marsman, M.; Hummer, K.; Kresse, G. Screened Hybrid Density Functionals Applied to Solids. *J. Chem. Phys.* **2006**, *124*, 154709.

(179) Paier, J.; Marsman, M.; Kresse, G. Why Does the B3LYP Hybrid Functional Fail for Metals? *J. Chem. Phys.* **2007**, *127*, 024103.

(180) Polo, V.; Kraka, E.; Cremer, D. Electron Correlation and the Self-Interaction Error of Density Functional Theory. *Mol. Phys.* **2002**, *100*, 1771–1790.

(181) Sharada, S. M.; Bligaard, T.; Luntz, A. C.; Kroes, G.-J.; Nørskov, J. K. SBH10: A

Benchmark Database of Barrier Heights on Transition Metal Surfaces. *J. Phys. Chem. C* **2017**, *121*, 19807–19815.

(182) Zheng, H.; Govoni, M.; Galli, G. Dielectric-Dependent Hybrid Functionals for Heterogeneous Materials. *Phys. Rev. Mater.* **2019**, *3*, 073803.

(183) Schmidt, P. S.; Thygesen, K. S. Benchmark Database of Transition Metal Surface and Adsorption Energies from Many-Body Perturbation Theory. *J. Phys. Chem. C* **2018**, *122*, 4381–4390.

(184) Golze, D.; Dvorak, M.; Rinke, P. The GW Compendium: A Practical Guide to Theoretical Photoemission Spectroscopy. *Front. Chem.* **2019**, *7*, 377.

(185) Ren, X.; Rinke, P.; Joas, C.; Scheffler, M. Random-Phase Approximation and its Applications in Computational Chemistry and Materials Science. *J. Mat. Sci.* **2012**, *47*, 7447–7471.

(186) Olsen, T.; Patrick, C. E.; Bates, J. E.; Ruzsinszky, A.; Thygesen, K. S. Beyond the RPA and GW Methods With Adiabatic XC-Kernels for Accurate Ground State and Quasiparticle Energies. *npj Comput. Mater.* **2019**, *5*, 106.

(187) Szabo, A.; Ostlund, N. S. *Modern Quantum Chemistry: Introduction to Advanced Electronic Structure Theory*; Dover Publications: Mineola, N.Y, 1996.

(188) Gaggioli, C. A.; Stoneburner, S. J.; Cramer, C. J.; Gagliardi, L. Beyond Density Functional Theory: The Multiconfigurational Approach To Model Heterogeneous Catalysis. *ACS Catalysis* **2019**, *9*, 8481–8502.

(189) Gagliardi, L.; Truhlar, D. G.; Manni, G. L.; Carlson, R. K.; Hoyer, C. E.; Bao, J. L. Multiconfiguration Pair-Density Functional Theory: A New Way To Treat Strongly Correlated Systems. *Acc. Chem. Res.* **2017**, *50*, 66–73.

(190) Toulouse, J.; Assaraf, R.; Umrigar, C. J. In *Electron Correlation in Molecules – Ab Initio Beyond Gaussian Quantum Chemistry*; Hoggan, P. E., Ozdogan, T., Eds.; Advances in Quantum Chemistry; Academic Press, 2016; Vol. 73; pp 285–314.

(191) Booth, G. H.; Grüneis, A.; Kresse, G.; Alavi, A. Towards an Exact Description of Electronic Wavefunctions in Real Solids. *Nature* **2013**, *493*, 365–370.

(192) Saritas, K.; Mueller, T.; Wagner, L.; Grossman, J. C. Investigation of a Quantum Monte Carlo Protocol To Achieve High Accuracy and High-Throughput Materials Formation Energies. *J. Chem. Theory Comput.* **2017**, *13*, 1943–1951.

(193) Dubecký, M.; Mitas, L.; Jurečka, P. Noncovalent Interactions by Quantum Monte Carlo. *Chem. Rev.* **2016**, *116*, 5188–5215.

(194) Pozzo, M.; Alfè, D. Hydrogen Dissociation on Mg(0001) Studied via Quantum Monte Carlo Calculations. *Phys. Rev. B* **2008**, *78*, 245313.

(195) Doblhoff-Dier, K.; Meyer, J.; Hoggan, P. E.; Kroes, G.-J. Quantum Monte Carlo Calculations on a Benchmark Molecule–Metal Surface Reaction: H2 + Cu(111). *J. Chem. Theory Comput.* **2017**, *13*, 3208–3219.

(196) Powell, A. D.; Kroes, G.-J.; Doblhoff-Diera, K. Quantum Monte Carlo Calculations on Dissociative Chemisorption of H2 + Al(110): Minimum Barrier Heights and Their Comparison to DFT Values. *J. Chem. Phys.* **2020**, *153*, 224701.

(197) Sharma, R. O.; Rantala, T. T.; Hoggan, P. E. Quantum Monte Carlo Approach for Determining the Activation Barrier of Water Addition to Carbon Monoxide Adsorbed on Pt(111) within 1 kJ/mol. *J. Phys. Chem. C* **2020**, *124*, 26232–26240.

(198) Hsing, C.-R.; Chang, C.-M.; Cheng, C.; Wei, C.-M. Quantum Monte Carlo Studies of CO Adsorption on Transition Metal Surfaces. *J. Phys. Chem. C* **2019**, *123*, 15659–15664.

(199) Sharma, R. O.; Rantala, T. T.; Hoggan, P. E. Selective Hydrogen Production at Pt(111) Investigated by Quantum Monte Carlo Methods for Metal Catalysis. *Int. J. Quantum Chem.* **2020**, *120*.

(200) Kent, P. R. C.; Annaberdiyev, A.; Benali, A.; Bennett, M. C.; Borda, E. J. L.; Doak, P.; Hao, H.; Jordan, K. D.; Krogel, J. T.; Kylänpää, I. et al. QMCPACK: Advances in the Development, Efficiency, and Application of Auxiliary Field and Real-Space Variational and Diffusion Quantum Monte Carlo. *J. Chem. Phys.* **2020**, *152*, 174105.

(201) Krogel, J. T.; Kent, P. R. C. Magnitude of Pseudopotential Localization Errors in Fixed Node Diffusion Quantum Monte Carlo. *J. Chem. Phys.* **2017**, *146*, 244101.

(202) Zen, A.; Brandenburg, J. G.; Michaelides, A.; Alfè, D. A New Scheme for Fixed Node Diffusion Quantum Monte Carlo With Pseudopotentials: Improving Reproducibility and Reducing the Trial-Wave-Function Bias. *J. Chem. Phys.* **2019**, *151*, 134105.

(203) Amovilli, C.; Filippi, C.; Floris, F. M. Coupling Quantum Monte Carlo to a Nonlinear Polarizable Continuum Model for Spherical Solutes. *J. Chem. Phys.* **2006**, *110*, 26225–26231.

(204) Schwarz, K. A.; Sundararaman, R.; Letchworth-Weaver, K.; Arias, T. A.; Hennig, R. G. Framework for Solvation in Quantum Monte Carlo. *Phys. Rev. B* **2012**, *85*, 201102(R).

(205) Sundararaman, R.; Schwarz, K.; Letchworth-Weaver, K.; Arias, T. A. Spicing up Continuum Solvation Models with SaLSA: the Spherically-Averaged Liquid Susceptibility Ansatz. *J. Chem. Phys.* **2015**, *142*, 054102.

(206) Jones, L. O.; Mosquera, M. A.; Schatz, G. C.; Ratner, M. A. Embedding Methods for Quantum Chemistry: Applications from Materials to Life Sciences. *J. Am. Chem. Soc.* **2020**, *142*, 3281–3295.

(207) Govind, N.; Wang, Y. A.; da Silva, A. J. R.; Carter, E. A. Accurate Ab Initio Energetics of Extended Systems via Explicit Correlation Embedded in a Density Functional Environment. *Chem. Phys. Lett.* **1998**, *295*, 129–134.

(208) Huang, C.; Pavone, M.; Carter, E. A. Quantum Mechanical Embedding Theory Based on a Unique Embedding Potential. *J. Chem. Phys.* **2011**, *134*, 154110.

(209) Schäfer, T.; Libisch, F.; Kresse, G.; Grüneis, A. Local Embedding of Coupled Cluster Theory Into the Random Phase Approximation Using Plane Waves. *J. Chem. Phys.* **2021**, *154*, 011101.

(210) Sun, Q.; Chan, G. K.-L. Quantum Embedding Theories. *Acc. Chem. Res.* **2016**, *49*, 2705–2712.

(211) Doblhoff-Dier, K.; Kroes, G.-J.; Libisch, F. Density Functional Embedding for Periodic and Nonperiodic Diffusion Monte Carlo Calculations. *Phys. Rev. B* **2018**, *98*, 085138.

(212) Petras, H. R.; Graham, D. S.; Ramadugu, S. K.; Goodpaster, J. D.; Shepherd, J. J. Fully Quantum Embedding with Density Functional Theory for Full Configuration Interaction Quantum Monte Carlo. *J. Chem. Theory Comput.* **2019**, *15*, 5332–5342.

(213) Reuter, K.; Stampf, C.; Scheffler, M. In *Handbook of Materials Modeling*; S., Y., Ed.; Springer: Dordrecht, 2005.

(214) Curtarolo, S.; Setyawan, W.; Hart, G. L.; Jahnatek, M.; Chepulskii, R. V.; Taylor, R. H.; Wang, S.; Xue, J.; Yang, K.; Levy, O. et al. AFLOW: An Automatic Framework for High-Throughput Materials Discovery. *Comput. Mater. Sci.* **2012**, *58*, 218.

(215) Jain, A.; Ong, S. P.; Hautier, G.; Chen, W.; Richards, W. D.; Dacek, S.; Cholia, S.; Gunter, D.; Skinner, D.; Ceder, G. et al. Commentary: The Materials Project: A

Materials Genome Approach to Accelerating Materials Innovation. *APL Mater.* **2013**, *1*, 011002.

(216) Groom, C. R.; Bruno, I. J.; Lightfoot, M. P.; Ward, S. C. The Cambridge Structural Database. *Acta Cryst.* **2016**, *B72*, 171–179.

(217) Winther, K. T.; Hoffmann, M. J.; Boes, J. R.; Mamun, O.; Bajdich, M.; Bligaard, T. Catalysis-Hub.org, An Open Electronic Structure Database for Surface Reactions. *Sci. Data* **2019**, *6*, 75.

(218) Ulissi, Z. W.; Singh, A. R.; Tsai, C.; Nørskov, J. K. Automated Discovery and Construction of Surface Phase Diagrams Using Machine Learning. *J. Phys. Chem. Lett.* **2016**, *7*, 3931–3935.

(219) Zhu, Q.; Li, L.; Oganov, A. R.; Allen, P. B. Evolutionary Method for Predicting Surface Reconstructions With Variable Stoichiometry. *Phys. Rev. B* **2013**, *87*, 195317.

(220) Wexler, R. B.; Qiu, T.; Rappe, A. M. Automatic Prediction of Surface Phase Diagrams Using Ab Initio Grand Canonical Monte Carlo. *J. Phys. Chem. C* **2019**, *123*, 2321–2328.

(221) Kitchin, J. R.; Reuter, K.; Scheffler, M. Alloy Surface Segregation in Reactive Environments: First-Principles Atomistic Thermodynamics Study of $Ag_3Pd(111)$ in Oxygen Atmospheres. *Phys. Rev. B* **2008**, *77*, 075437.

(222) Tang, H. Phase Diagram of Oxygen Adsorbed on Platinum (111) by First-Principles Investigation. *Phys. Rev. B* **2004**, *70*, 045420.

(223) Weitzner, S. E.; Dabo, I. Voltage-Dependent Cluster Expansion for Electrified Solid-Liquid Interfaces: Application to the Electrochemical Deposition of Transition Metals. *Phys. Rev. B* **2017**, *96*, 205134.

(224) Lym, J.; Gu, G. H.; Jung, Y.; Vlachos, D. G. Lattice Convolutional Neural Network Modeling of Adsorbate Coverage Effects. *J. Phys. Chem. C* **2019**, *123*, 18951–18959.

(225) Groenenboom, M. C.; Moffat, T. P.; Schwarz, K. A. Halide-Induced Step Faceting and Dissolution Energetics from Atomistic Machine Learned Potentials on Cu(100). *J. Phys. Chem. C* **2020**, *124*, 12359–12369.

(226) Boes, J. R.; Kitchin, J. R. Neural Network Predictions of Oxygen Interactions on a Dynamic Pd Surface. *Surf. Chem.* **2017**, *43*, 346–354.

(227) Ulissi, Z. W.; Tang, M. T.; Xiao, J.; Liu, X.; Torelli, D. A.; Karamad, M.; Cummins, K.; Hahn, C.; Lewis, N. S.; Jaramillo, T. F. et al. Machine-Learning Methods Enable Exhaustive Searches for Active Bimetallic Facets and Reveal Active Site Motifs for CO2 Reduction. *ACS Catal.* **2017**, *7*, 6600–6608.

(228) Schwarz, K.; Groenenboom, M. C.; Moffat, T. P.; Sundararaman, R.; Vinson, J. Resolving the Geometry/Charge Puzzle of the c(2 x 2)-Cl Cu(100) Electrode. *J. Phys. Chem. Lett.* **2021**, *12*, 440–446.

(229) Li, X.-Y.; Chen, A.; Yang, X.-H.; Zhu, J.-X.; Le, J.-B.; Cheng, J. Linear Correlation between Water Adsorption Energies and Volta Potential Differences for Metal/water Interfaces. *J. Phys. Chem. Lett.* **2021**, *12*, 7299–7304.

(230) Ludwig, T.; Gauthier, J. A.; Brown, K. S.; Ringe, S.; Nørskov, J. K.; Chan, K. Solvent–Adsorbate Interactions and Adsorbate-Specific Solvent Structure in Carbon Dioxide Reduction on a Stepped Cu Surface. *J. Phys. Chem. C* **2019**, *123*, 5999–6009.

(231) Heenen, H. H.; Gauthier, J. A.; Kristoffersen, H. H.; Ludwig, T.; Chan, K. Solvation at Metal/Water Interfaces: An Ab Initio Molecular Dynamics Benchmark of Common Computational Approaches. *J. Chem. Phys.* **2020**, *152*, 144703.

(232) Zhang, J.; Glezakou, V.-A.; Rousseau, R.; Nguyen, M.-T. NWPEsSe: An Adaptive-Learning Global Optimization Algorithm for Nanosized Cluster Systems. *J. Chem. Theory Comput.* **2020**, *16*, 3947–3958.

(233) Pratt, L. R.; Rempe, S. B. Quasi-Chemical Theory and Implicit Solvent Models for Simulations. *AIP Conf. Proc.* **1999**, *492*, 172–201.

(234) López, A. C. D.; Eggert, T.; Reuter, K.; Hörmann, N. G. Static and Dynamic Water Structures at Interfaces: A Case Study With Focus on Pt(111). *J. Chem. Phys.* **2021**, *155*, 194702.

(235) Sundararaman, R.; Schwarz, K. Evaluating Continuum Solvation Models for the Electrode-Electrolyte Interface: Challenges and Strategies for Improvement. *J. Chem. Phys.* **2017**, *146*, 084111.

(236) Petrosyan, S. A.; Briere, J.-F.; Roundy, D.; Arias, T. A. Joint Density-functional Theory for Electronic Structure of Solvated Systems. *Phys. Rev. B* **2007**, *75*, 205105.

(237) Plaza, M.; Huang, X.; Ko, J. Y. P.; Shen, M.; Simpson, B. H.; Rodríguez-López, J.; Ritzert, N. L.; Letchworth-Weaver, K.; Gunceler, D.; Schlom, D. G. et al. Structure of the Photo-catalytically Active Surface of $SrTiO_3$. *J. Amer. Chem. Soc.* **2016**, *138*, 7816–7819.

(238) Sundararaman, R.; Letchworth-Weaver, K.; Schwarz, K. A.; Gunceler, D.; Ozhabes, Y.; Arias, T. JDFTx: Software for Joint Density-functional Theory. *SoftwareX* **2017**, *6*, 278 – 284.

(239) Sundararaman, R.; Arias, T. Efficient Classical Density-functional Theories of Rigid-molecular Fluids and a Simplified Free Energy Functional for Liquid Water. *Comp. Phys. Comm.* **2014**, *185*, 818.

(240) Sundararaman, R.; Letchworth-Weaver, K.; Arias, T. A. A Recipe for Free-Energy Functionals of Polarizable Molecular Fluids. *J. Chem. Phys.* **2014**, *140*, 144504.

(241) Chandler, D.; McCoy, J.; Singer, S. Density Functional Theory of Nonuniform Polyatomic Systems. I. General Formulation. *J. Chem. Phys.* **1986**, *85*, 5971.

(242) Chandler, D.; McCoy, J.; Singer, S. Density Functional Theory of Nonuniform Polyatomic Systems. II. Rational Closures for Integral Equations. *J. Chem. Phys.* **1986**, *85*, 5978.

(243) Otani, M.; Sugino, O. First-principles Calculations of Charged Surfaces and Interfaces: A Plane-wave Nonrepeated Slab Approach. *Phys. Rev. B* **2006**, *73*, 115407.

(244) Nishihara, S.; Otani, M. Hybrid Solvation Models for Bulk, Interface, and Membrane: Reference Interaction Site Methods Coupled with Density Functional Theory. *Phys. Rev.B* **2017**, *96*, 115429.

(245) Simm, G. N.; Türtscher, P. L.; Reiher, M. Systematic Microsolvation Approach With a Cluster-Continuum Scheme and Conformational Sampling. *J. Comp. Chem.* **2020**, *41*, 1144–1155.

(246) Tang, E.; Tommaso, D. D.; de Leeuw, N. H. Accuracy of the Microsolvation–Continuum Approach in Computing the pKa and the Free Energies of Formation of Phosphate Species in Aqueous Solution. *Phys. Chem. Chem. Phys.* **2010**, *12*, 13804–13815.

(247) Roldan, A. Frontiers in First Principles Modelling of Electrochemical Simulations. *Curr. Opin. Electrochem.* **2018**, *10*, 1–6.

(248) Sundararaman, R.; Goddard, W. The Charge-Asymmetric Nonlocally-Determined Local-Electric (CANDLE) Solvation Model. *J. Chem. Phys* **2015**, *142*, 064107.

(249) Andreussi, O.; Hörmann, N. G.; Nattino, F.; Fisicaro, G.; Goedecker, S.; Marzari, N. Solvent-Aware Interfaces in Continuum Solvation. *J. Chem. Theory Comput.* **2019**, *15*, 1996–2009.

(250) Maurer, P.; Laio, A.; Hugosson, H. W.; Colombo, M. C.; Rothlisberger, U. Automated Parametrization of Biomolecular Force Fields from Quantum Mechanics/Molecular Mechanics (QM/MM) Simulations through Force Matching. *J. Chem. Theory Comput.* **2007**, *3*, 628–639.

(251) Izvekov, S.; Parrinello, M.; Burnham, C. J.; Voth, G. A. Effective Force Fields for Condensed Phase Systems From Ab Initio Molecular Dynamics Simulation: A New Method for Force- Matching. *J. Chem. Phys.* **2004**, *120*, 10896.

(252) Norskov, J. K.; Rossmeisl, J.; Logadottir, A.; Lindqvist, L.; Kitchin, J. R.; Bligaard, T.; Jonsson, H. Origin of the Overpotential for Oxygen Reduction at a Fuel-Cell Cathode. *J. Phys. Chem. B* **2004**, *108*, 17886–17892.

(253) Karlberg, G. S.; Rossmeisl, J.; Norskov, J. K. Estimations of Electric Field Effects on the Oxygen Reduction Reaction Based on the Density Functional Theory. *Phys. Chem. Chem. Phys.* **2007**, *9*, 5158–5161.

(254) Chen, L. D.; Urushihara, M.; Chan, K.; Norskov, J. K. Electric Field Effects in Electrochemical CO2 Reduction. *ACS Catalysis* **2016**, *6*, 7133–7139.

(255) Chan, K.; Nørskov, J. K. Electrochemical Barriers Made Simple. *J. Phys. Chem. Lett.* **2015**, *6*, 2663–2668.

(256) Hörmann, N. G.; Marzari, N.; Reuter, K. Electrosorption at Metal Surfaces From First Principles. *npj Comput. Mater.* **2020**, *6*, 136.

(257) Gauthier, J. A.; Dickens, C. F.; Ringe, S.; Chan, K. Practical Considerations for

Continuum Models Applied to Surface Electrochemistry. *ChemPhysChem* **2019**, *20*, 3074–3080.

(258) Gauthier, J. A.; Ringe, S.; Dickens, C. F.; Garza, A. J.; Bell, A. T.; Head-Gordon, M.; Nørskov, J. K.; Chan, K. Challenges in Modeling Electrochemical Reaction Energetics with Polarizable Continuum Models. *ACS Catalysis* **2019**, *9*, 920–931.

(259) Gauthier, J. A.; Dickens, C. F.; Heenen, H. H.; Vijay, S.; Ringe, S.; Chan, K. Unified Approach to Implicit and Explicit Solvent Simulations of Electrochemical Reaction Energetics. *J. Chem. Theory Comput.* **2019**, *15*, 6895–6906.

(260) Hörmann, N. G.; Andreussi, O.; Marzari, N. Grand Canonical Simulations of Electrochemical Interfaces in Implicit Solvation Models. *J. Chem. Phys.* **2019**, *150*.

(261) Chen, X.; McCrum, I. T.; Schwarz, K. A.; Janik, M. J.; Koper, M. T. M. Co-adsorption of Cations as the Cause of the Apparent pH Dependence of Hydrogen Adsorption on a Stepped Platinum Single-Crystal Electrode. *Angew. Chem. Int. Ed.* **2017**, *56*, 15025–15029.

(262) Valette, G. Double Layer on Silver Single Crystal Electrodes in Contact With Electrolytes Having Anions Which are Slightly Specifically Adsorbed: Part II. The (100) Face. *J. Electroanal. Chem. Interf. Electrochem.* **1982**, *138*, 37–54.

(263) Dupont, C.; Andreussi, O.; Marzari, N. Self-Consistent Continuum Solvation (SCCS): the Case of Charged Systems. *J. Chem. Phys* **2013**, *139*, 214110.

(264) Weaver, M. J. Potentials of Zero Charge for Platinum(111)-Aqueous Interfaces: A Combined Assessment from In-Situ and Ultrahigh-Vacuum Measurements. *Langmuir* **1998**, *14*, 3932–3936.

(265) Westphal, D.; Goldmann, A. Chlorine Adsorption on Copper: II. Photoemission From Cu(001)c(2 x 2)-C1 and Cu(111)($\sqrt{3}$ x $\sqrt{3}$)R30°. *Surf. Sci.* **1983**, *131*, 113–138.

(266) Gartland, P.; Berge, S.; Slagsvold, B. Photoelectric Work Function of a Copper Single Crystal for the (100), (110), (111), and (112) Faces. *Phys. Rev. Lett.* **1972**, *28*, 738.

(267) G.Liu,; Zou, S.; Josell, D.; Richter, L.; Moffat, T. SEIRAS Study of Chloride Mediated Polyether Adsorption on Cu. *J. Phys. Chem. C* **2018**, *122*, 21933–21951.

(268) C.Figueiredo, M.; Hiltrop, D.; Sundararaman, R.; A.Schwarz, K.; T.M.Koper, M. Absence of Diffuse Double Layer Effect on the Vibrational Properties and Oxidation of Chemisorbed Carbon Monoxide on a Pt(111) Electrode. *Electrochim. Acta* **2018**, *281*, 127 – 132.

(269) Wang, J.; Li, C.; Shin, S.; Qi, H. Accelerated Atomic Data Production in Ab Initio Molecular Dynamics with Recurrent Neural Network for Materials Research. *J. Phys. Chem. C* **2020**, *124*, 14838–14846.

(270) Tsai, S.-T.; Kuo, E.-J.; Tiwary, P. Learning Molecular Dynamics With Simple Language Model Built Upon Long Short-Term Memory Neural Network. *Nat. Commun.* **2020**, *11*, 5155.